Glass Europe Vol. 3 (2025) 45-75
https://doi.org/10.52825/glass-europe.v3i.2519

Submitted: 19 Oct. 2024 | Accepted: 14 Apr. 2025 | Published: 08 May 2025

Iron-Doped Magnesium Aluminosilicate Transparent Glass-Ceramics. Mg-Petalite or Spinel Nanocrystals? Competing Mechanisms

Vasilisa Bukina[1], Olga Dymshits[1,*], Irina Alekseeva[1], Anna Volokitina[1], Maksim Tenevich[2], Anastasia Bachina[2], and Aleksandr Zhilin[3]

[1]S.I. Vavilov State Optical Institute, St Petersburg, Russia

[2]Ioffe Institute, St Petersburg, Russia

[3]D.V. Efremov Institute of Electrophysical Apparatus, St Petersburg, Russia

*Correspondence: Olga Dymshits, vodym1959@gmail.com

Abstract. Transparent glass-ceramics based on Fe^{2+}:Mg-petalite and/or Fe^{2+}:$MgAl_2O_4$ nanocrystals were obtained from the initial glass by single and two-stage heat-treatments at temperatures from 800 to 1000 °C. $ZrTiO_4$ and spinel crystallized during the DSC scan up to 1000 °C. Spinel nanocrystals 9-12 nm in size also appeared during single and two-stage heat-treatments at temperatures of 850 - 1000 °C. Mg-petalite crystallites ~30 nm in size evolved in the narrow temperature range from 850 to 900 °C during single-stage holding periods. A maximum fraction of Mg-petalite crystallized at 850 °C. Once formed, Mg-petalite is preserved upon further heating and holding even at 1000 °C for 6 h. Mg-petalite and spinel transformed into sapphirine and highly siliceous residual glass during heating at 1100 °C. Competing crystallization mechanisms are discussed. In materials with a weakly developed liquid-liquid phase-separated structure, crystallization of Mg-petalite from the magnesium aluminosilicate glass predominates, and spinel becomes an additional phase. Spinel crystallizes as the main phase from glasses with the developed liquid-liquid phase-separated structure. Its crystallization is accompanied by the formation of highly siliceous glass, from which Mg-petalite crystallization is impossible. Intense absorption band with maximum at ~1.9 μm due to fourfold coordinated Fe^{2+} ions in spinel nanocrystals is used as a spectral indicator of spinel formation. Glass-ceramics are relevant for the development of saturable absorbers intended for lasers operating at 1.6-2.4 μm.

Keywords: Mg-Petalite, Spinel, Ferrous Ions, Transparent Glass-Ceramics, Nucleating Agents, Nanocrystals

1. Introduction

Petalite, a lithium aluminosilicate with the formula $LiAlSi_4O_{10}$, is a rare mineral, which was found and first described by d'Andrada in 1801 [1]. It is a commercially important ore for Li recovery. Petalite crystallizes in a monoclinic crystallographic system and has the space group P2/a [2]. It can be considered either as a layered silicate with a structure built of folded $[Si_4O_{10}]$ layers connected by AlO_4 and LiO_4 tetrahedra or as a three-dimensional framework of corner-shared LiO_4, AlO_4 and SiO_4 tetrahedra [3]. According to Černý and London [4], the stability field of petalite is limited by β-spodumene at high temperatures and by eucryptite at low temperatures and pressure. Recently, glass-ceramics based on petalite and lithium silicates were developed [5].

In 1961, Schreyer and Schairer [6] described surface crystallization of a metastable phase with a petalite structure that crystallized along with other phases from the magnesium aluminosilicate glass with the composition (wt%) 20.5 MgO, 17.5 Al_2O_3, 62 SiO_2 by the heat-treatment at 900 °C for up to 5 days. Its X-ray pattern resembled that of the petalite, $LiAlSi_4O_{10}$, and lithium disilicate, while its composition was located in the region of the excess content of MgO over Al_2O_3 in the triangle between $MgO{\cdot}2SiO_2$, $MgO{\cdot}Al_2O_3{\cdot}3SiO_2$ and $MgO{\cdot}Al_2O_3{\cdot}8SiO_2$ [7]. It is interesting to note that, according to ref. [7], in spite of the similarity with petalite, Mg-petalite was never obtained from any composition having equimolar contents of MgO and Al_2O_3. The main difficulty in characterization of the physical properties of Mg-petalite is that it always crystallizes accompanied by other crystalline phases and often by a residual glass [7].

Addition of nucleating agents (ZrO_2, TiO_2, their mixture, MoO_3, and/or WO_3) changes the mechanism of crystallization of Mg-petalite and promotes its volume crystallization [8-18]. It is worth mentioning that, in this case, compositions of initial glasses can lie not only in the composition range suggested by Schreyer and Schairer [7] but also along the line SiO_2 – spinel, and even to the right of this line in the mullite crystallization field, in the region of the excess content of Al_2O_3 over MgO.

For instance, with the addition of ZrO_2 as a nucleating agent, Mg-petalite crystallizes in glasses that belong to the silica - cordierite join [8-10]. Holmquist [8] reported that crystallization of Mg-petalite was enhanced in glasses with compositions $MgO{\cdot}Al_2O_3{\cdot}nSiO_2$ as the silica content increases. Indeed, the glass with the composition 90 wt% ($MgO{\cdot}Al_2O_3{\cdot}4.3\ SiO_2$) + 10 wt% ZrO_2 heat-treated at 845 °C for 70 h contained only Mg-petalite and ZrO_2 nanocrystals. The β-quartz solid solution appeared in the material at 1000 °C during holding for 2 h, and the transformation to β-quartz solid solution was irreversible. This finding was confirmed by Conrad [9], who studied one of the glasses suggested by Holmquist [8], with the composition $MgO{\cdot}Al_2O_3{\cdot}3SiO_2$, and demonstrated that at low temperatures and long times of heat-treatments Mg-petalite evolved after crystallization of tetragonal ZrO_2. Alekseeva *et al.* [10] studied phase transformations in the glass of the same base composition, also nucleated by ZrO_2, and observed the crystallization of Mg-petalite along with β-quartz solid solutions during the heat-treatment at 850 °C for 48 h. Mg-petalite decomposed with the formation of β-quartz solid solutions and spinel. The authors noted that spinel crystallized only in those glass-ceramics that earlier contained Mg-petalite [10].

The mechanism of liquid-liquid phase separation in glasses nucleated by TiO_2, resulting in three-phase immiscibility and crystallization of Mg-petalite, was suggested by Varshal *et al.* [11]. Glass compositions yielding Mg-petalite during heat-treatments at early stages of glass transformations at 900 – 1000 °C were found in the region with a high content of MgO and low content of SiO_2 near the liquid-liquid phase separation field. This region is similar to the region of glass compositions described by Schreyer and Schairer [7]. Varshal *et al.* [11] considered Mg-petalite as a solid solution formed as a result of the substitution of $2Si^{4+}$ by $2Al^{3+} + Mg^{2+}$ in the layered silicate structure or due to the incorporation of $(AlO_4)Mg_{0.5}$ groups between silicate layers.

Pinkney and Beall [12] described the crystallization of Mg-petalite and a $MgTi_2O_5$ solid solution in the titania-containing glass with the composition (wt%) 15 MgO, 1.8 ZnO, 24.8 Al_2O_3, 46.9 SiO_2 nucleated by 11.5 TiO_2 during its heat-treatment at 850 °C for 30 min. The phase composition of glass-ceramics obtained at higher temperatures included also spinel and a β-quartz solid solution.

Bortkevich *et al.* [13] described the crystallization of Mg-petalite with crystal sizes ranging from 23 to 60 nm in glass-ceramics of the magnesium aluminosilicate system with excess content of MgO over Al_2O_3, nucleated by TiO_2 and obtained by heat-treatments in the temperature range from 850 to 950 °C for 6 h. In these materials, the crystallization of Mg-petalite was accompanied by magnesium aluminotitanates, spinel and enstatite. Mg-petalite did not crystallize in glass-ceramics obtained by heat-treatments in the same temperature range from

glasses with the same silica content located in the mullite crystallization field [13]. Only traces of Mg-petalite were found in glass-ceramics obtained from the glass located on the SiO_2 – cordierite join and heat-treated at the second stage at 950 °C [13].

Mg-petalite also crystallizes in magnesium aluminosilicate glasses containing mixed nucleating agents, TiO_2 and ZrO_2. Barry *et al.* [14] have studied the effect of the TiO_2/ZrO_2 ratio on phase transformations in glass with the cordierite composition. They demonstrated that formation of Mg-petalite depends on the preceding phase separation and, therefore, on the content and ratio of nucleating agents, being the greatest for the equimolar ratio of TiO_2 and ZrO_2. Mg-petalite was assigned a composition $MgO{\cdot}Al_2O_3{\cdot}3SiO_2$. It was found to decompose to nanocrystals of β-quartz solid solution, cordierite and cristobalite upon heat-treatment at 1050 °C.

Buch *et al.* [15] obtained transparent glass-ceramics nucleated by a mixture of 6 mol% TiO_2 and 3.2 mol% ZrO_2, containing Mg-petalite as the major phase, with β-quartz solid solution and ZrO_2 as minor phases, by two-stage heat-treatments of glass with the composition (mol%) 21.9 MgO, 19.7 Al_2O_3, 49.1 SiO_2. Suggesting that the mechanism of liquid-liquid phase-separation resulted in crystallization of these phases, the authors referred to the findings of Varshal *et al.* [11].

Early stages of phase transformations in a glass with composition close to cordierite nucleated by ZrO_2 and TiO_2 were also investigated by Lembke *at al.* [16]. According to ref. [16], large Mg-petalite crystals appeared during heat-treatment at 820 °C for 4 h, followed by crystallization of high-quartz (i.e., β-quartz) solid solution and ZrO_2 as the heat-treatment time was increased beyond 6 h. Lembke *at al.* [16] also determined the stoichiometry of Mg-petalite as $MgO{\cdot}Al_2O_3{\cdot}3SiO_2$. This stoichiometry was previously predicted by Schreyer and Schairer as a result of substitution of Mg + Al for Li + Si [7]. It is also in accordance with findings of ref. [14].

Carl *et al.* [17] studied phase transformations in a glass with an alumina excess over MgO nucleated by ~5 mol% TiO_2 and ~3 mol% ZrO_2 using single and two-stage heat-treatments. Besides $ZrTiO_4$, they detected Mg-petalite crystallization during single-stage heat-treatment at 850 °C. The maximum crystallization of Mg-petalite occurred during the heat-treatment at 875 °C, accompanied by β-quartz solid solution.

Recently, crystallization of Mg-petalite with sizes of about 100 μm was observed in the glass of the model composition 20 MgO, 20 Al_2O_3, 60 SiO_2 (wt%) containing 0.8 wt% WO_3 and melted under reducing conditions [18].

From the literature mentioned above, devoted to the crystallization of Mg-petalite in glasses of the magnesium aluminosilicate system, one may conclude that the mechanisms and kinetics of phase separation, as well as the phase assemblage of the resulting glass-ceramics, depend on the composition of the initial glass, the nature and amount of the nucleating agent and the heat-treatment schedule.

Recently, we have developed transparent spinel-based glass-ceramics doped with Fe^{2+} ions and nucleated by TiO_2 [19] and a mixture of TiO_2 and ZrO_2 [20]. We proposed them as possible saturable absorbers for nanosecond lasers working in the spectral range of 1.8–2.4 μm. These eye-safe lasers find applications in medicine and meteorology, in range finding and remote sensing, in gas analysis, etc. When we studied the formation of transparent glass-ceramics based on Fe^{2+}:$MgAl_2O_4$ nanocrystals nucleated by a mixture of TiO_2 and ZrO_2 using two-stage heat-treatments, traces of Mg-petalite were found in the glass-ceramic prepared by the heat-treatment at 800 °C for 6 h + 850 °C for 6 h [20]. The aim of the present research is to study the conditions of Mg-petalite crystallization in the same initial glass and the properties of the Mg-petalite-based glass-ceramics. The mechanisms resulting in crystallizations of Mg-petalite and spinel are discussed.

2. Experimental

2.1 Sample preparation

The model glass of the same composition as studied by Holmquist [8] and Conrad [9], i.e., 20 MgO, 20 Al_2O_3, 60 SiO_2 (mol%), was nucleated by a mixture of 5 mol% TiO_2 and 5 mol% ZrO_2 [20], and doped with 0.6 mol% FeO. The raw materials were reagent grade oxides. The glass melting procedure was described elsewhere [20]. The image of the transparent yellow-colored glass is shown in Fig. 1.

The glass was subjected to single and two-stage heat-treatments in a Nabertherm muffle furnace in the temperature range from 800 to 1100 °C with a heating rate of 5 K min^{-1} and holding times from 0 to 24 h. After the heat-treatment, the samples were either cooled as the furnace cooled, or quenched and allowed to cool to room temperature. Their color changed with the heat-treatment temperature from yellow to deep brown. An increase of the holding time at 850 °C from 6 to 24 h led to a deeper brown coloration. For the two-stage heat-treatments, the first stage was either at 800 °C, or at 850 °C for 6 h. As a result, transparent glass-ceramics were obtained by all heat-treatments (Fig. 1).

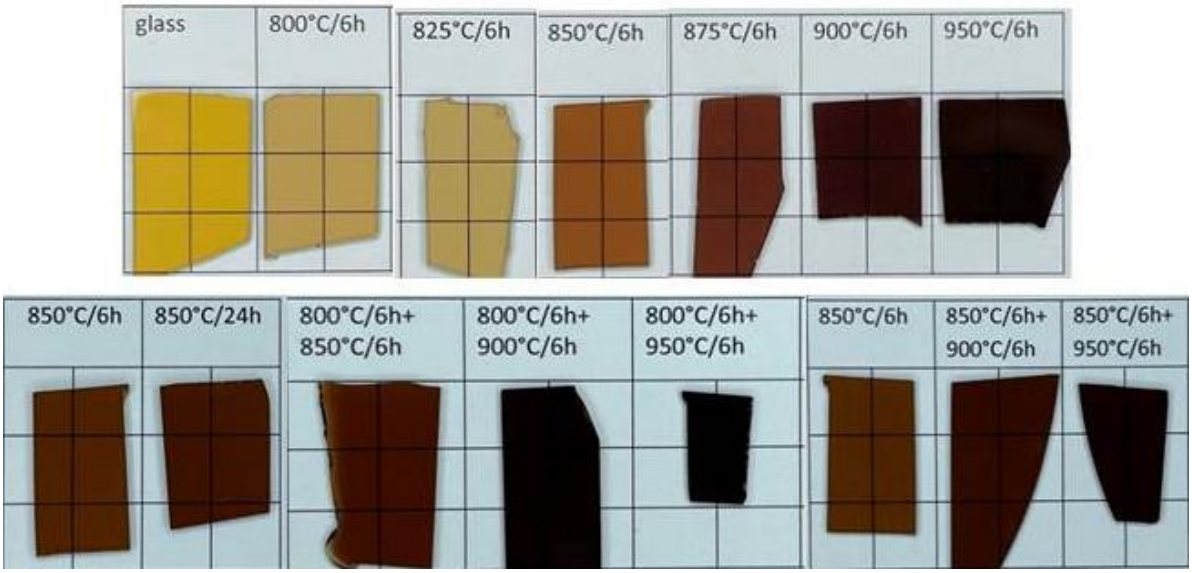

Figure 1. *Photographs of the polished samples with thickness of ~1 mm. The heat-treatment schedules (°C/h) are written above corresponding images.*

2.2. Methods

Powder XRD patterns were obtained using a diffractometer Shimadzu XRD-6000 with Ni filtered Cu Kα radiation (λ = 1.5406 Å). The mean crystallite sizes were calculated according to Scherrer's equation (1) [21]

$$D_{XRD} = \frac{K\lambda}{\Delta \cdot \cos\theta} \quad (1)$$

where *K* is the constant assumed to be 1 [21], *λ* is the wavelength of the X-ray radiation, Δ is the width of the peak at half of its maximum, and *θ* is the diffraction angle. The error in determining the mean crystallite size depends on their size and equals 5-10%. The mean size of $ZrTiO_4$ nanocrystals was estimated from the peak with Miller's indices *(hkl)* = (111), while the mean size of spinel was estimated from the peak with indices (440). The indexing of XRD patterns of Mg-petalite nanocrystals was made according to the data given in the ICDD

card #75–1716 for Li-petalite, space group P2/a. The mean size of Mg-petalite nanocrystals was estimated from the peak with indices *(hkl)* = (002).

The spinel unit cell parameter *a* was estimated from the position of the (440) peak with an error of ±0.003 Å. The unit cell parameters *a, b,* and *c* of Mg-petalite were estimated from the positions of the (002), (400) and (020) peaks, respectively, with an error of ±0.02 Å. The *β* angle was determined from the $(21\bar{1})$, (211), $(11\bar{2})$, and (112) peaks with an error of ±0.1°. The unit cell parameters *a, b,* and *c* of sapphirine (space group $P2_1/a$) were estimated from the positions of the (200), (002) and (040) peaks, respectively. The *β* angle was determined from the $(11\bar{4})$ and (114) peaks with an error of ±0.1°. The unit cell volumes of Mg-petalite and sapphirine were determined by the equation $V = a \cdot b \cdot c \cdot \sin\beta$.

A NETZSCH STA 449 F3 Jupiter simultaneous thermal analyzer with a dynamic Ar flow atmosphere was used for the study by differential scanning calorimetry (DSC). Bulk samples of the initial and heat-treated glass with a weight of about 15 mg were used. The heating rates were 5 and 10 K min^{-1}.

Raman spectra were acquired in backscattering geometry on an InVia (Renishaw, England) Micro-Raman spectrometer with a multichannel detector cooled up to -70 °C. The samples were polished plates with a thickness of ~1 mm. The spectra were excited by Ar^+ CW laser line at 488 nm. A laser power of 0.5 mW was used, which allowed obtaining high-quality spectra without causing local structural changes in the sample. Leica 50× (N.A. = 0.75) objective was used to illuminate the sample and collect scattered light. An edge filter was used. Each spectrum, ranging from 60 to 1400 cm^{-1}, was averaged over 30 acquisitions with duration of 10 s. The spatial resolution was of 2 cm^{-1}.

Optical absorption spectra were recorded on a Shimadzu UV-3600 spectrophotometer in the spectral range from 200 to 3300 nm. The samples were the same polished plates with a thickness of ~1 mm that were used for Raman spectra recording. The absorption coefficient *α* was estimated taking into account light losses.

The morphology of the samples was studied by Tescan Vega 3 SBH scanning electron microscope (SEM). Before the study, the surface of the aforementioned polished samples was etched in a hydrofluoric acid for ~2 s and washed in distilled water in an ultrasonic bath.

Densities of the initial and heat-treated glasses were determined by the toluene displacement method. The experimental error was within ±0.0005 g.cm^{-3}.

Linseis model L 75 VS 1000 dilatometer was used to measure the coefficients of thermal expansion of the initial and heat-treated glasses from room temperature to 330 °C at a heating rate of 5 °C·min^{-1}. The samples were rods with a length from 40 to 50 mm and a square section of ~4×4 mm. The error in estimating the coefficients of thermal expansion was ±2%.

3. Results

3.1. Differential Scanning Calorimetry, DSC

The heat flow DSC signal of the initial glass as a function of temperature (heating rate 10 K min^{-1}) is shown in Fig. 2. The glass transition temperature, T_g, is 765 °C. Three exothermic peaks are observed on the DSC curve in the selected temperature range. Their crystallization onset temperatures, T_{on}, not shown in the figure, are T_{on1} = 843 °C, T_{on2} = 925 °C, and T_{on3} = 1055 °C. Their maximum crystallization temperatures, T_{max}, are T_{max1}=870 °C, T_{max2}= 959 °C and T_{max3}=1086 °C. The exothermic peak at 959 °C is more intensive and sharper than the other peaks.

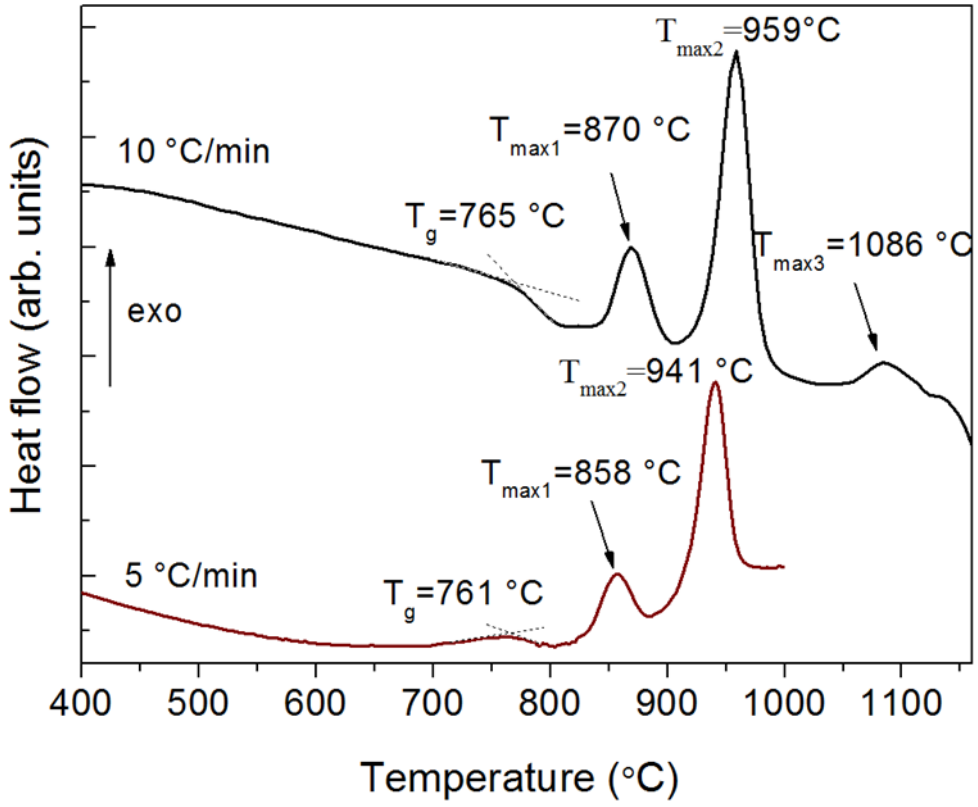

Figure 2. *DSC curves of the quenched glass. The heating rates are 5 and 10 K·min^{-1}. T_g stands for the glass transition temperature, T_{max} stands for the maximum crystallization temperature.*

In ref. [20], we have found that crystallization of zirconium titanate, $ZrTiO_4$, with an orthorhombic structure, is responsible for the appearance of the first peak on the heat flow curve, while the second peak is caused by crystallization of spinel with a cubic structure, and the third peak is associated with appearance of sapphirine.

3.2 X-ray diffraction, XRD

Fig. 3a shows XRD patterns of the initial glass and glass subjected to single-stage heat-treatments at temperatures from 800 to 950 °C for 6 h. The initial glass is X-ray amorphous. Nanocrystals of the nucleating agent, $ZrTiO_4$, ~6 nm in size, appear in glass heat-treated at 800 and 825 °C (Table 1). The position of the amorphous halo does not change and remains at $2\theta \simeq 24.3$ °, the same value as in the XRD pattern of the initial glass. XRD patterns of all glass-ceramics prepared in the temperature range from 850 to 950 °C contain peaks of $ZrTiO_4$ crystallites, with mean sizes increasing from ~6.0 to ~7.2 nm, and spinel with sizes ranging from 9.5 to 11.8 nm (Fig. 3a and Table 1). The spinel unit cell parameter *a* increased from 8.068 Å to 8.091 Å with increasing the heat-treatment temperature from 850 to 950 °C (Table 1).

Mg-petalite crystallizes during isothermal holdings in the temperature range from 850 to 900 °C, while the XRD pattern of the sample obtained by the heat-treatment at 950 °C does not show peaks assigned to Mg-petalite. The maximum intensity of Mg-petalite peaks is observed in the XRD pattern of the sample obtained by the heat-treatment at 850 °C for 6 h (Fig. 3a). The size of Mg-petalite crystallites is ~29 nm (Table 1). The unit cell parameters of Mg-petalite are listed in Table 2. As a result of this heat-treatment, the amorphous halo disappears, which indicates a high degree of volume crystallization of the magnesium aluminosilicate glass matrix.

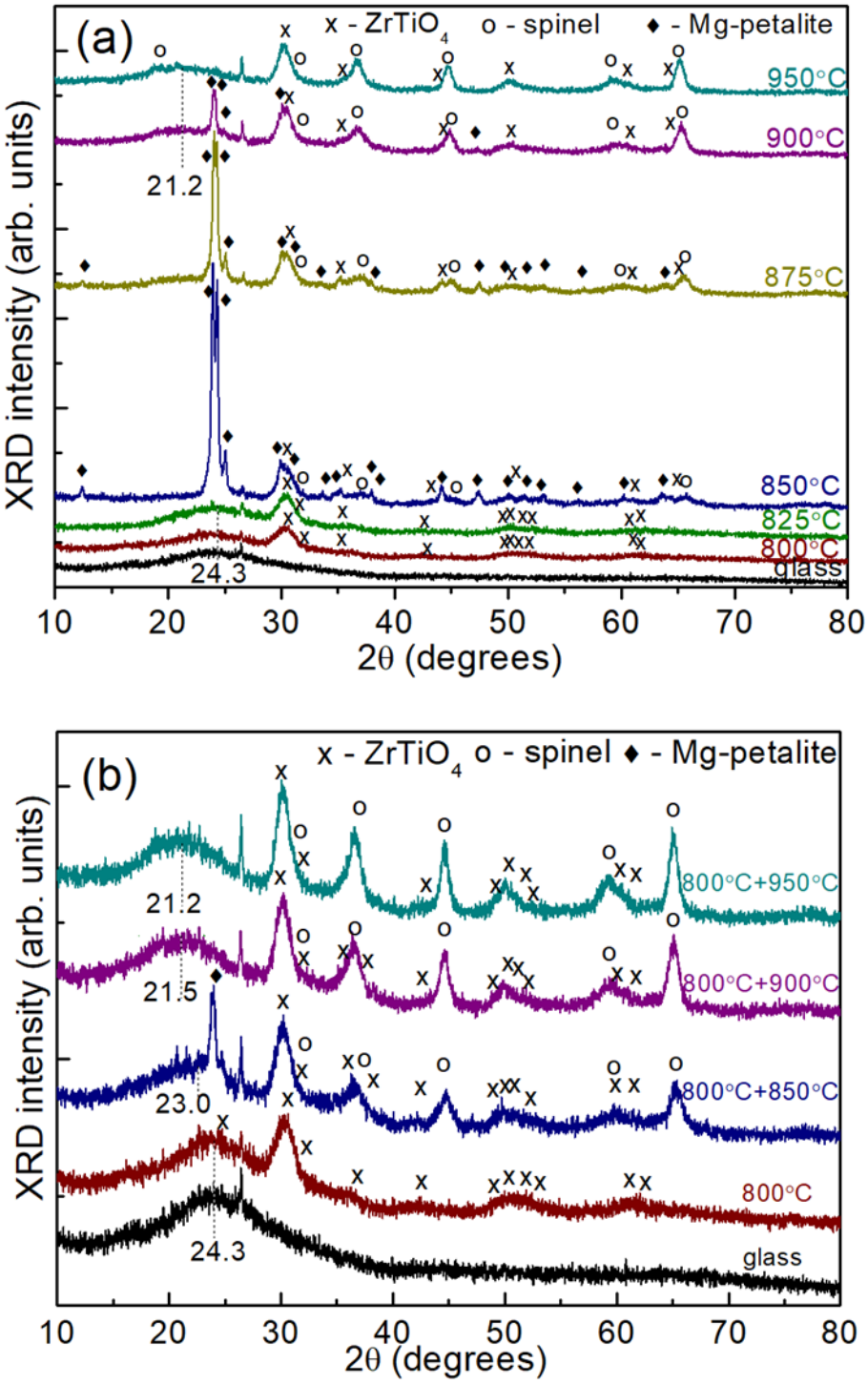

Figure 3. *XRD patterns of the initial glass and glass-ceramics obtained by single-stage (a) and two-stage (b) heat-treatments. The values 800-950 °C indicate the temperature of heat-treatment, the duration of which is 6 h at each stage. The dashed lines show the position of the maximum of the amorphous halo.*

With increasing the heat-treatment temperature from 850 to 900 °C, the intensity of the Mg-petalite peaks decreases, while the mean size of crystallites remains nearly unchanged (Table 1). The spinel crystallinity fraction increases accompanied by the amorphous halo of the residual glass with the maximum at 2θ = 21.2 ° (Fig. 3a). The spinel crystallite sizes remain near constant and equal to 9.5 - 9.8 nm (Table 1).

In the XRD pattern of the sample heat-treated at 950 °C, only spinel nanocrystals with a mean size of 11.8 nm and $ZrTiO_4$ nanocrystals with a mean size of 7.2 nm are found (Table 1). The maximum of the amorphous halo of the residual glass is at 2θ = 21.2 °, which is similar to the maximum of the amorphous halo in silica glass. The similar position of the amorphous halo was always obtained in the XRD patterns of glass-ceramics of magnesium and zinc aluminosilicate systems based on nanocrystals with spinel structure [19], [20], [22], [23].

The phase assemblage of glass-ceramics obtained by two-stage heat-treatments with the first hold at 800 °C for 6 h is strikingly different. In these glass-ceramics, spinel is the main crystalline phase [20] (Fig. 3b and Tables 1 and 3). A small amount of Mg-petalite is found only in the glass-ceramic obtained by the second stage heat-treatment at 850 °C for 6 h [20]. The gradual shift of the position of the maximum of the amorphous halo of the residual glass to the value of 2θ=21.2 ° is clearly seen.

Table 1. *Mean size, D, of $ZrTiO_4$, Mg-petalite and spinel nanocrystals and spinel unit cell parameter a in glass-ceramics prepared by single and two-stage heat-treatments in the temperature range from 800 to 1000 °C.*

Heat-treatment schedule	**$ZrTiO_4$**	**Mg-petalite**	**Spinel**		**Reference**
	D, nm	**D, nm**	**D, nm**	***a*, Å**	
800 °C, 6 h	6.0	-	-	-	[20]
825 °C, 6 h	6.0	-	-	-	-
850 °C, 0 h	4.5	-	-	-	-
850 °C, 6 h	6.2	29.0	9.5	-	-
875 °C, 6 h	6.9	28.5	9.5	-	-
900 °C, 0 h	5.8	-	-	-	-
900 °C, 6 h	7.0	29.3	9.8	8.078	-
950 °C, 0 h	6.5	-	10.0	8.084	-
950 °C, 6 h	7.2	-	11.8	8.091	-
800 °C, 6 h+850 °C, 6 h	6.0	16.0	8.5	8.068	[20]
800 °C, 6 h+900 °C, 6 h	6.5	-	9.5	8.098	[20]
800 °C, 6 h+950 °C, 6 h	8.0	-	12.0	8.099	[20]
850 °C, 6 h+900 °C, 6 h	6.5	28.7	6.4	8.073	-
850 °C, 6 h+950 °C, 6 h	7.5	29.2	9.5	8.084	-
850 °C, 6 h+1000 °C, 6 h	11.5	29.5	14.0	8.091	-

The crystallization of Mg-petalite during single-stage heat-treatments seems to contradict the results of the DSC study, as the DSC curve of the quenched glass does not show any exothermic peak that can be assigned to Mg-petalite. In the attempt to reveal its crystallization by the DSC method, we performed the DSC scan at the heating rate of 5 $K \cdot min^{-1}$ (Fig. 2). As expected, this resulted in decreasing the characteristic glass transition and crystallization temperatures of the already observed peaks, but no additional peaks that could be associated with Mg-petalite crystallization was detected.

To resolve this contradiction and follow the Mg-petalite crystallization at 850 °C, we made single-stage heat-treatments at 850 °C with durations from 0 to 24 h (Fig. 4, where an asterisk denotes XRD patterns of samples quenched from the hot furnace; Table 3). At 850 °C, only $ZrTiO_4$ crystallizes in the glass when it is quenched from the hot furnace. This is consistent with the DSC results presented in Fig. 2, where the first exothermic peak (T_{on1} = 843 °C) is attributed to crystallization of $ZrTiO_4$ [20].

Table 2. *The parameters a, b, c, β angle, and volume of Mg-petalite and sapphirine unit cells and their mean crystallite sizes in glass-ceramics.*

Heat-treatment schedule, °C/h	***a*, Å**	***b*, Å**	***c*, Å**	***β*, °**	**V, Å^3**	**D, nm**	**Crystalline phase**
850/3	11.57	5.11	7.75	112.4	423.7	21.0	Mg-petalite
850/6	11.50	5.18	7.67	112.1	423.3	29.0	Mg-petalite
850/24	11.62	5.12	7.71	112.7	423.2	23.3	Mg-petalite
875/6	11.60	5.10	7.69	112.5	420.3	28.5	Mg-petalite
850/6+900/6	11.65	5.11	7.70	112.7	422.9	26.5	Mg-petalite
850/6+950/6	11.66	5.08	7.62	112.7	416.4	26.2	Mg-petalite
850/6+1000/6	11.73	5.06	7.60	113.2	414.6	29.5	Mg-petalite
850/6+1100/6	11.69	13.94	10.40	128.3	1330.0	28.0	sapphirine

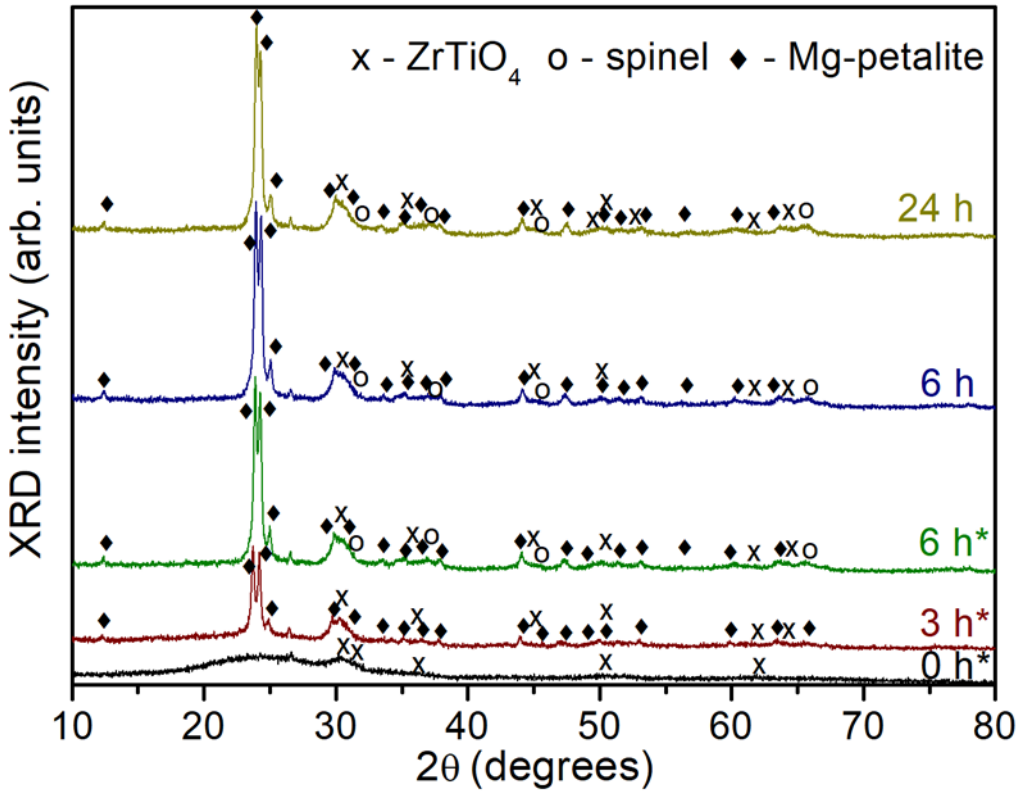

Figure 4. *XRD patterns of samples heat-treated at 850 °C for 0 to 24 h. Asterisk denotes XRD patterns of samples quenched from the hot furnace.*

Mg-petalite crystallites, ~21 nm in size, evolve during holding at 850 °C for 3 h. The maximum Mg-petalite crystallinity fraction is reached after 6 h, with crystal size reaching 29 nm, as it was mentioned above. Note that spinel nanocrystals are also seen in this XRD pattern. Increasing the holding time to 24 h does not change the phase assemblage of glass-ceramic, which remains composed of Mg-petalite, $ZrTiO_4$, and spinel with mean crystallite sizes of 23.3, 6.2 and 9.0 nm, respectively (Table 3).

A closer examination of the peaks of Mg-petalite with Miller's indices (210) and (201), located in the angular range 2θ from 23 to 25 °, reveals that after a 24 h heat-treatment the peaks with indices (210) and (201) get closer; a shift is observed where the peak (210) moves towards larger angles and the peak (201) shifts towards smaller angles (not shown here). This change in the peaks positions is caused by variations in the unit cell parameters (Table 2). The

prolonged heat-treatment results in increasing the *a* and *c* parameters and *β* angle and decreasing the *b* parameter. It should be mentioned that the peaks of Mg-petalite located in the 2θ range from 23 to 25 ° have somewhat different intensities.

Table 3. *Mean sizes, D, of crystallites in glass-ceramics prepared by the single-stage heat-treatment in the temperature range from 800 to 950 °C for 6 h*

Heat-treatment schedule	D, nm		
	$ZrTiO_4$	Mg-petalite	Spinel
850 °C, 3 h	6.0	21.0	-
850 °C, 6 h	6.2	29.0	9.5
850 °C, 24 h	6.2	23.3	9.0

We have not only studied the conditions for the formation of Mg-petalite nanocrystals, but also their structural transformations with increasing the heat-treatment temperature. For this purpose, the glass that underwent heat-treatment at 850 °C for 6 h and contained Mg-petalite nanocrystals was subjected to additional heat-treatments ranging from 900 to 1100 °C. The XRD patterns of these samples are shown in Fig. 5a,b. Increasing the heat-treatment temperature up to 1000 °C resulted in a sluggish decomposition of Mg-petalite and an increase in the spinel fraction. Heat-treatment at 1100 °C led to the transformation of Mg-petalite and spinel into sapphirine and residual highly siliceous glass.

Note that the same phase assemblage is characteristic of the glass-ceramic obtained by the two-stage heat-treatment with the first hold at 800 °C for 6 h and the second hold at the same crystallization temperature of 1100 °C (Fig. 5a).

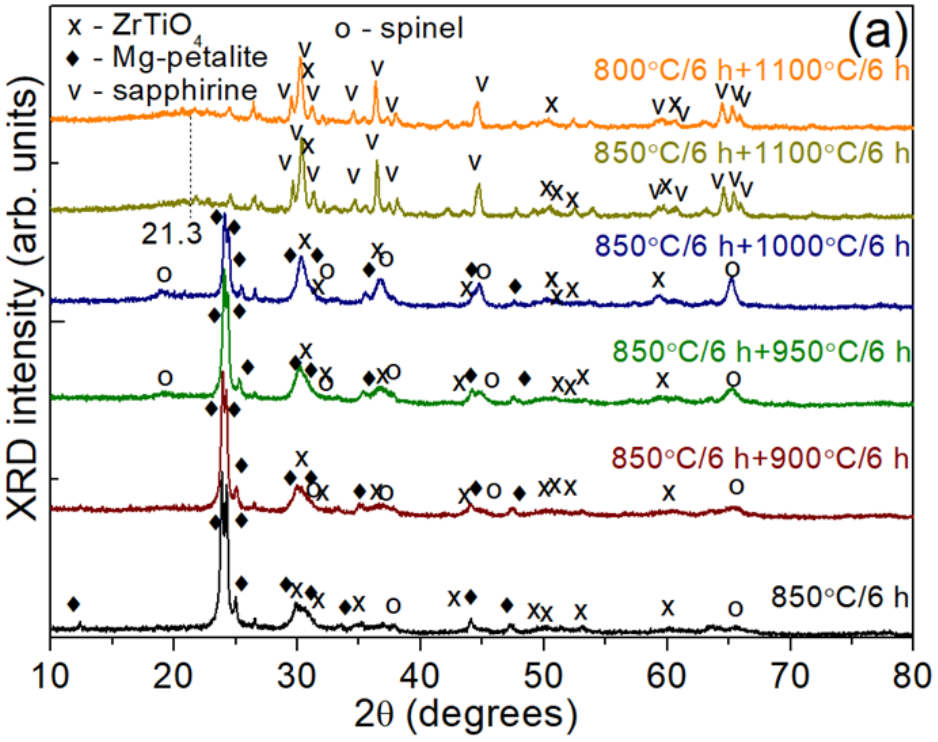

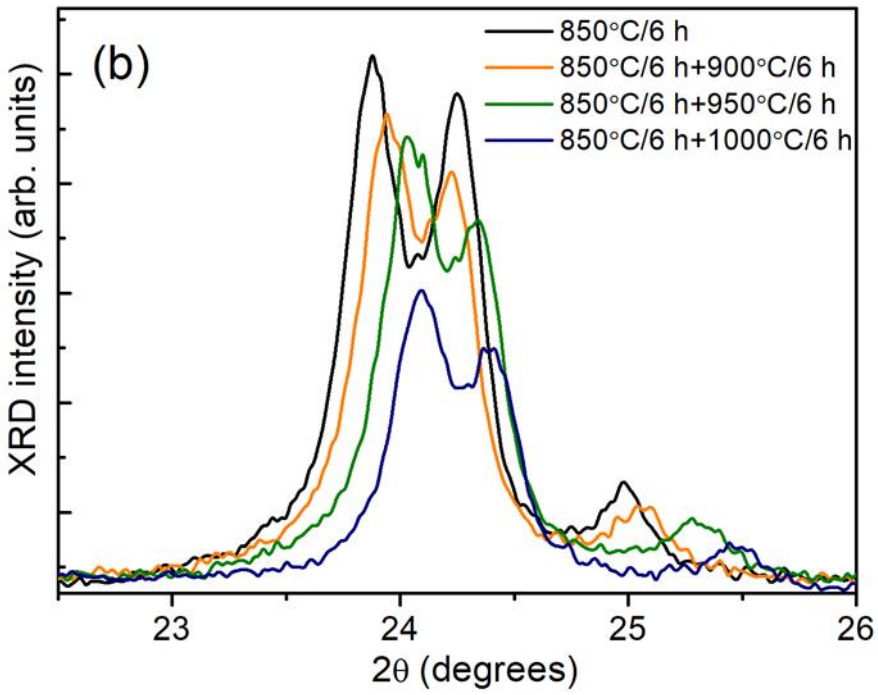

***Figure 5**. (a) XRD patterns of glass-ceramic obtained by heat-treatment at 850 °C for 6 h and additionally heat-treated at temperatures ranging from 900 to 1100 °C, and the XRD pattern of the sample heat-treated at 800 °C for 6 h + 1100 °C for 6 h. The patters are shifted for better observation. (b) A closer look on the main XRD peaks of Mg-petalite.*

Fig. 6 presents the DSC curves of the quenched glass and materials obtained by heat-treatments at 800 and at 850 °C for 6 h. As previously mentioned, the initial glass is X-ray amorphous, the glass heat-treated at 800 °C for 6 h contains nanocrystals of $ZrTiO_4$, and the

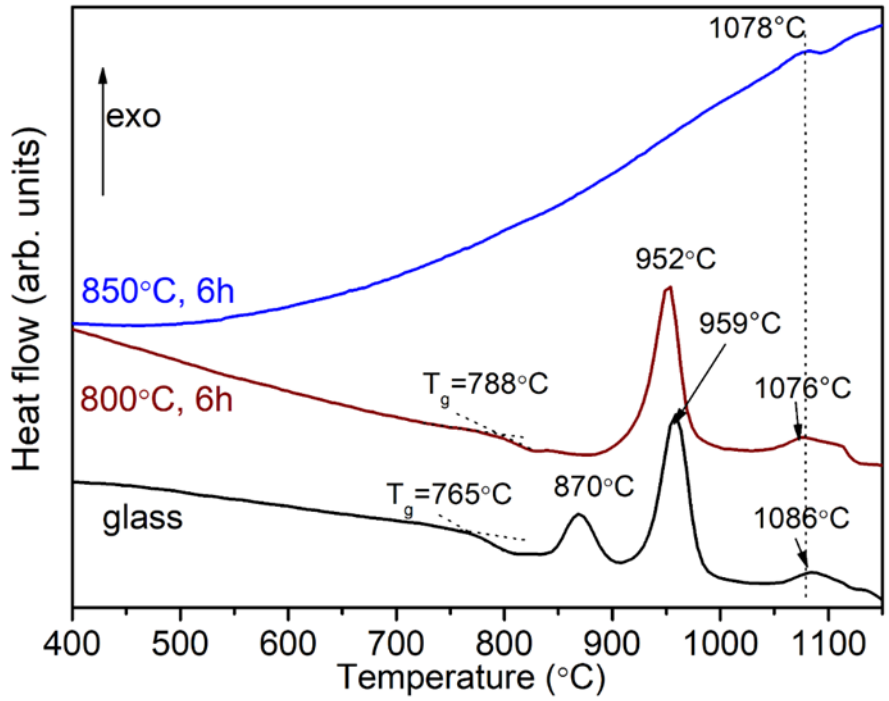

***Figure 6.** DSC curves of the quenched glass and the glass heat-treated at 800 and 850 °C for 6 h. The heating rate is 10 K·min-1. T_g stands for the glass transition temperature. The curves are shifted for better observation.*

glass heat-treated at 850 °C for 6 h contains nanocrystals of $ZrTiO_4$, Mg-petalite and spinel (Fig. 3a). There is no exothermic peak assigned to $ZrTiO_4$ with T_{max1} = 870 °C on the DSC curve of the sample heat-treated at the nucleation stage, as nearly all $ZrTiO_4$ had already crystallized during this heat-treatment [20]. The DSC curve of the sample heat-treated at 850 °C for 6 h is steep, suggesting that all $ZrTiO_4$ and spinel nanocrystals that crystallized during the heating of the initial glass in the DSC furnace were already formed by the heat-treatment at 850 °C for 6 h. The DSC curves of all materials have exothermic peak at ~1080 °C regardless of their phase composition (Fig. 6), which is assigned to sapphirine crystallization.

3.3 Raman spectroscopy

The Raman spectrum of the initial glass presented in Fig. 7 is rather similar to the spectrum of a glass of the same composition doped with NiO [24]. The difference is that the peak positions in the spectrum of the glass under study are slightly shifted towards higher wavenumbers. The spectrum shows broad high-wavenumber bands with maxima at ~805 and ~930 cm^{-1}, a tail with inflection at ~1100 cm^{-1}, and a broad middle-range band with a maximum at ~470 cm^{-1}. The band at ~930 cm^{-1} has the highest intensity. The assignment of the observed bands in the Raman spectrum of the similar glass was given elsewhere [24]. For our study, it is noteworthy that the high-wavenumber band is centered at ~930 cm^{-1}, which is different from its position at ~920 cm^{-1} in the Raman spectrum of the same glass doped solely by TiO_2 [19]. This difference can be an indirect evidence of the localization of zirconium ions near titanium ions in the initial glass, similar to the observation made by Dugué *et al.* [24].

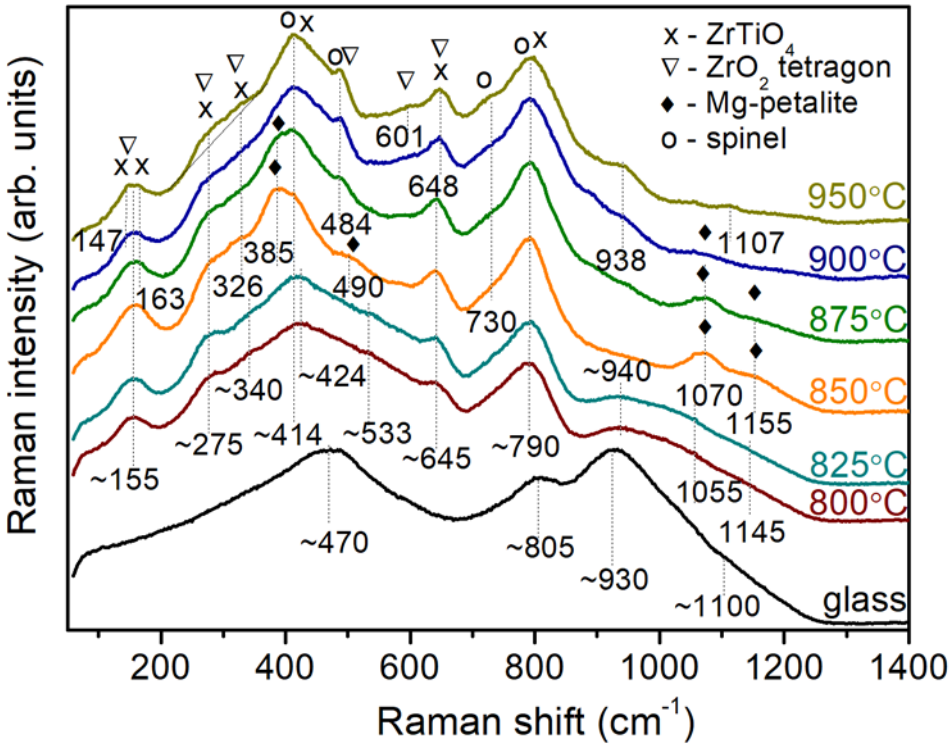

Figure 7. *Raman spectra of the initial glass and transparent glass-ceramics obtained by single-stage heat-treatments, between 800-950 °C for a duration of 6 h, using the excitation wavelength at 488 nm. Numbers denote positions of the Raman peaks in cm^{-1}. The curves are shifted for better observation.*

The Raman spectra change after heat-treatment at the nucleation stage (800 °C for 6 h). The intensity of the band at 930 cm^{-1} decreases while a new band appears at ~790 cm^{-1}. The band at ~805 cm^{-1} is hardly discernible. The main middle-range band is concealed within the broad band with a maximum at ~424 cm^{-1} (Fig. 7). A weak broad band, with barely pronounced maxima at ~940, ~1055 and ~1145 cm^{-1}, is found in the high-wavenumber region. Bands at ~155, ~275, ~340, ~414, ~533, and ~645 cm^{-1} are also present. All these bands, including the

one at ~790 cm^{-1}, can be assigned to $ZrTiO_4$ nanocrystals according to refs [25], [26], where Raman bands of tetragonal $ZrTiO_4$ have peaks at 154-158, ~269, ~331, ~415, ~539, ~590, ~646 and ~795 cm^{-1}, with the strongest at ~415, ~646 and ~795 cm^{-1}. Similar spectral features are seen in the spectrum of the sample prepared at 825 °C for 6 h. Note that both materials contain $ZrTiO_4$ nanocrystals, as confirmed by XRD data (Fig. 3a). Dugué *et al.* suggested that similar changes in the Raman spectrum not only indicate crystallization of $ZrTiO_4$, but also suggest the formation of an amorphous aluminotitanate phase, which, quite possibly, includes zirconium and magnesium ions [24].

After heat-treatments at 850 and 875°C for 6 h, there are changes in the middle- and high-wavenumber ranges of the spectrum. Raman bands characteristic of spinel nanocrystals with a partly inverse structure appear at ~414 and ~730 cm^{-1} [19]. Additionally, the main middle-range band becomes narrower with a pronounced maximum shifted to lower wavenumbers, while new bands appear at ~385, ~490, ~1070, and ~1155 cm^{-1}. We found these bands only in the Raman spectra of glass-ceramics containing Mg-petalite. They do not appear in the spectrum of glass-ceramic obtained by heat-treatment at 950 °C (Fig. 7), and, therefore, can be assigned to Mg-petalite nanocrystals. As we did not find Raman spectrum of Mg-petalite in literature, we had to compare our findings with the Raman spectrum of petalite. Unoriented Raman spectrum of petalite, $LiAlSi_4O_{10}$ [27], is presented in Fig. 8 together with the spectra of glass-ceramics obtained by heat-treatments at 850 °C for 6 and 24 h.

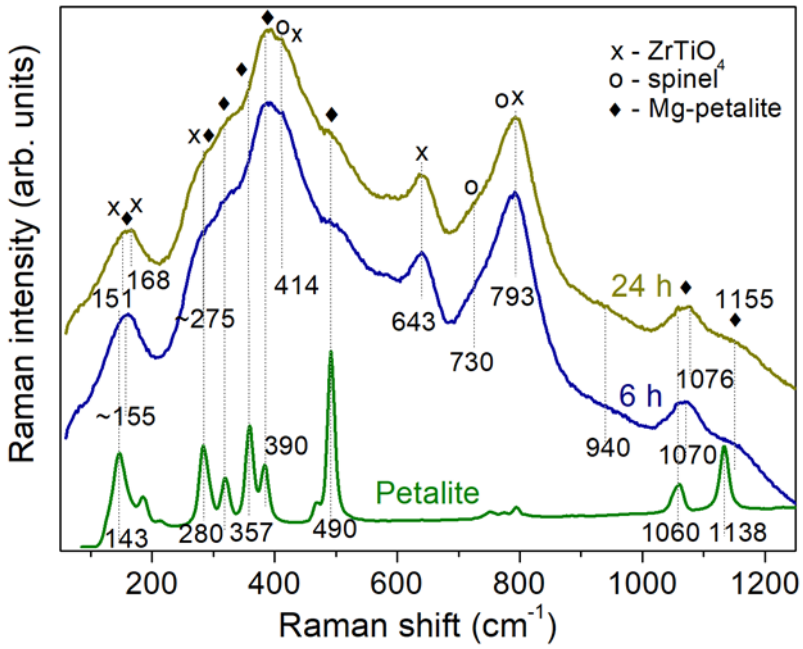

Figure 8. *Raman spectra of transparent glass-ceramics obtained by single-stage heat-treatments at 850 °C for 6 and 24 h, and the Raman spectrum of petalite [27], using excitation wavelengths are 488 and 532 nm, respectively. Labels 6 h and 24 h indicate the heat-treatment time. Numbers denote positions of the Raman peaks in cm^{-1}. The curves are shifted for better observation*.

The main Raman bands characteristic of petalite are located at ~490 and 357 cm^{-1} (with a satellite at 383 cm^{-1}) [28]. According to Kaminskii *et al.* [28], Raman bands in the range between 300 and 400 cm^{-1} correspond to bending vibrations of the SiO_4 and AlO_4 tetrahedra, with a very strong band at 357 cm^{-1} being assigned to asymmetric bending vibrations of (SiO_4/AlO_4) tetrahedra. The bands at 1138 and 1060 cm^{-1} were related to the symmetric and asymmetric stretching vibrations of the SiO_4 tetrahedra coupled with the symmetric (Si–O–Si) vibration. The strong band at 490 cm^{-1} was assigned to the symmetric bending vibrations of the SiO_4 tetrahedra. Therefore, it is not surprising that these bands are seen in the spectrum of glass-ceramics based on Mg-petalite, as it is an aluminosilicate with a similar structure (Figs 8 and 9).

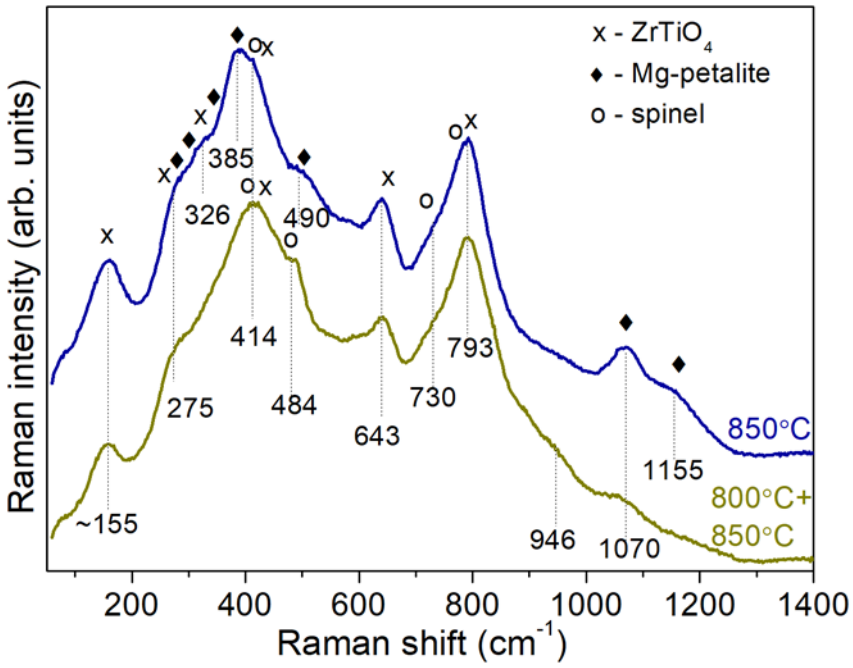

Figure 9. *Raman spectra of transparent glass-ceramics obtained by heat-treatments at 850 °C for 6 h by single and two stages. The excitation wavelength is 488 nm. Labels indicate the heat-treatment temperatures. Numbers denote positions of the Raman peaks in cm^{-1}. The curves are shifted for better observation.*

After identifying the bands assigned to vibrations of structural groupings in Mg-petalite nanocrystals in Raman spectra of glass-ceramics under study, we revisited the Raman spectra of magnesium aluminosilicate glass-ceramics nucleated by titania and containing Mg-petalite, which we studied several years ago [13]. As it turns out, these spectra also contain characteristic vibrations in the region of 375 and 490 cm^{-1}, which we had not notice earlier.

Fig. 9 shows Raman spectra of glass-ceramics prepared at 850 °C by single and two-stage heat-treatments. The peaks assigned to Mg-petalite in the Raman spectrum of the sample obtained by the single-stage heat-treatment at 850 °C are hardly seen in the spectrum of the sample obtained by two-stage heat-treatment, which contains spinel and $ZrTiO_4$ with traces of Mg-petalite (Fig. 3a,b and Fig. 9).

Raman spectra of glass-ceramics prepared at 900 and 950 °C for 6 h show bands that can be assigned to $ZrTiO_4$ nanocrystals and spinel nanocrystals with a partly inverse structure, located at 414, 484, 730, and 790 cm^{-1} [19]. In the glass-ceramic obtained at 950 °C, additional bands ascribed to tetragonal ZrO_2 [29] partly overlapp with the bands of $ZrTiO_4$ nanocrystals. The presence of tetragonal ZrO_2 together with $ZrTiO_4$ is difficult to confirm by XRD data because of the very close positions of their main peaks (2θ = 30.25 ° for ZrO_2 and 2θ = 30.60 ° for $ZrTiO_4$) and large widths due to the small crystal size. The broad bands of low intensity at ~938 and ~1107 cm^{-1} that appear in the Raman spectrum of the glass-ceramic prepared at 950 °C suggest that a small amount of titanium ions remains in the residual glass enriched in silica [30]. These spectra do not show Mg-petalite spectral features. Fig. 10 shows similarity between the Raman spectra of samples obtained by single- and two-stage heat-treatment at 950 °C for 6 h.

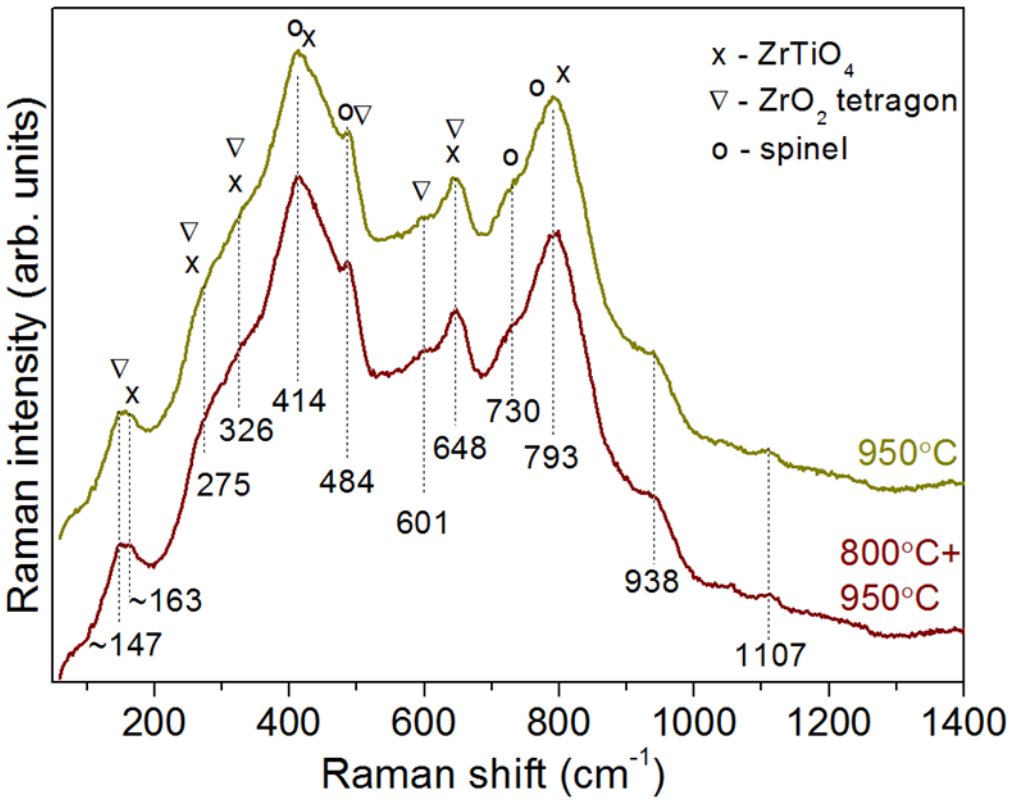

Figure 10. *Raman spectra of transparent glass-ceramics obtained by single- and two-stage heat-treatments at 950 °C for 6 h. λ_{exc} = 488 nm. Labels indicate the heat-treatment temperature. Numbers denote the position of the Raman peaks in cm^{-1}. The curves are shifted for better observation.*

3.4 The SEM study

Fig. 11 illustrates the evolution of the initial glass morphology as a function of the heat-treatment temperature by SEM analysis. In the SEM image of the initial glass (Fig. 11a) scattered regions with varying contrast are visible which may represent inhomogeneous regions with different compositions. According to XRD analysis, the material is amorphous; thus, the observed inhomogeneous structure may indicate liquid-liquid phase separation that occurred during glass casting, cooling and annealing. Bright particles unevenly dispersed across the glass surface are likely artifacts from the sample preparation process, specifically from surface etching and carbon deposition steps, and therefore were not considered.

Upon subjecting the glass to single-stage heat-treatments with increasing temperature, the morphology drastically changes. After heat-treatment at 800 °C, the SEM image reveals the presence of small particles, approximately 10±5 nm in size, homogeneously distributed along the field of view (Fig. 11b). The inhomogeneous structure of the material is difficult to explain only by the nanosized (~6 nm) $ZrTiO_4$ crystallites, as observed in the XRD data. It can be assumed that the formation of this structure is also due to the development of liquid-liquid phase separation that occurred in the initial glass, which precedes further phase transformations.

In the SEM image of the sample heat-treated at 850 °C for 6 h, agglomerated particles ranging from 20 to 100 nm in size are observed throughout the field of view (Fig. 11c). The large aggregates have an elongated shape. This may be indicative of the magnesium aluminosilicate glass crystallization, initiated by $ZrTiO_4$ nanocrystals serving as nucleating sites. According to XRD data, the crystallized phases at this temperature are Mg-petalite (~29 nm), $ZrTiO_4$ (~6 nm), and spinel (~9.5 nm), see Table 1.

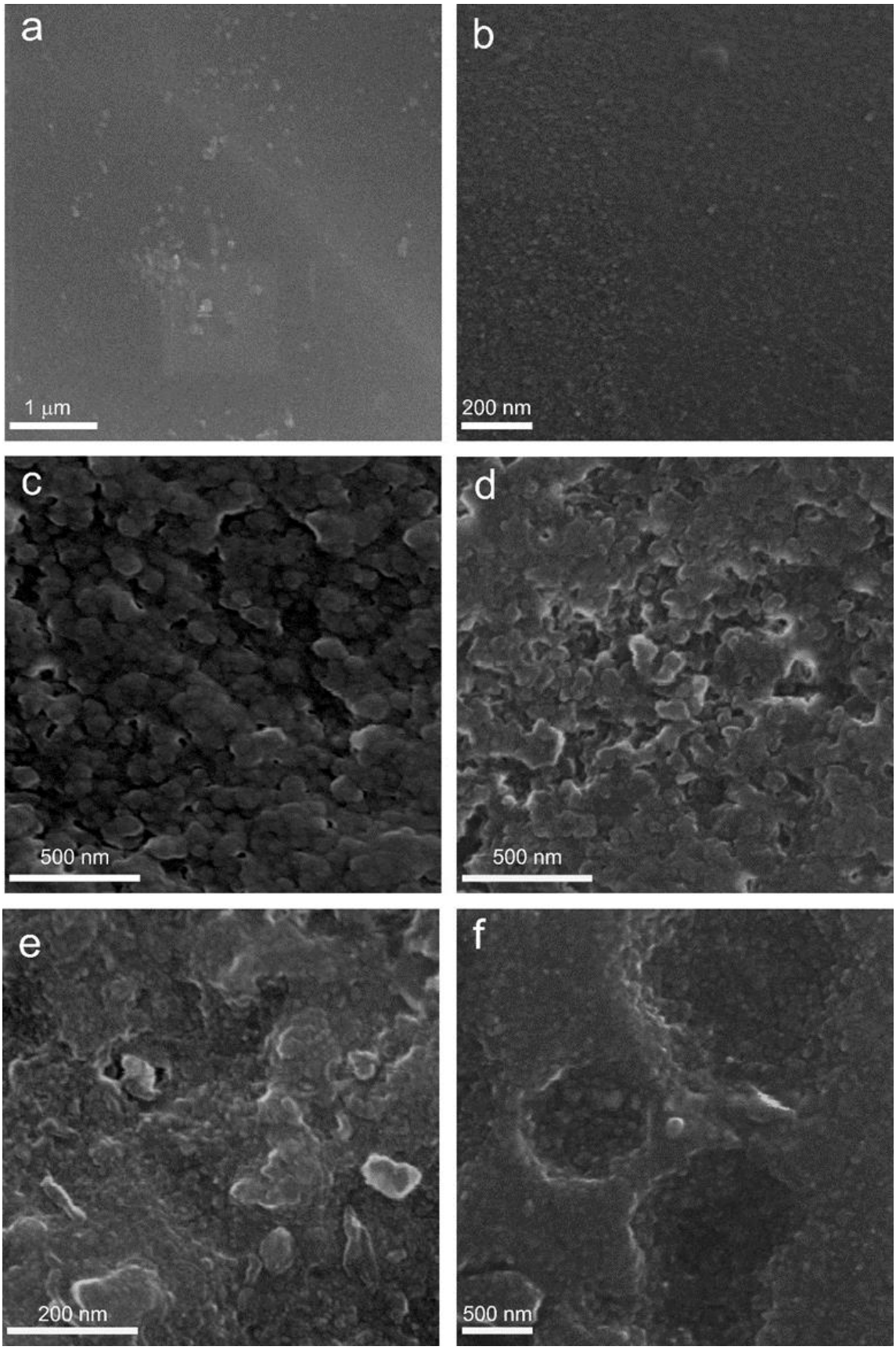

Figure 11. *SEM images of the samples: (a) initial glass, glasses heat-treated at (b) 800 °C for 6 h, (c) 850 °C for 6 h, (d) 850 °C for 24 h, (e) 900 °C for 6 h and (f) 950 °C for 6 h.*

The structures of the samples heat-treated at 850 °C for 6 and 24 h are similar. However, the extended heat-treatment time leads to further particle growth and a reduction of spaces between them Fig. 11c,d). According to the XRD data, the phase composition and crystallite sizes in both glass-ceramics are nearly the same. Probably these structural changes led to some increase in density of the glass-ceramic (Fig. 12).

As the heat-treatment temperature increases to 900 °C, the SEM image shows the formation of numerous small agglomerated particles approximately 15±5 nm in size, alongside with larger particles measuring approximately 60±15 nm (Fig. 11e). The smaller particles are likely the predominant crystalline phase, identified as spinel by XRD analysis, while the larger particles represent Mg-petalite. The number of these larger aggregates is small, which is consistent with the XRD data (Fig. 3a), indicating an insignificant content of Mg-petalite in this sample.

The SEM image of the glass-ceramic prepared by heat-treatment at 950 °C reveals agglomerated particles dispersed in the residual glass matrix. According to the XRD findings, these particles can be attributed to spinel nanocrystals. The large particles previously associated with the petalite-like magnesium aluminosilicate phase are no longer observed, which aligns with the XRD data. The caverns observed in the image are likely the result of etching of the residual silica-enriched glass (Fig. 11f).

3.5 Evaluation of density of the glass and glass-ceramics

Fig. 12a shows the dependence of density on the temperature of single-stage heat-treatments of the initial glass. The density of the initial glass is equal to 2.7279 g.cm^{-3}. After heat-treatments at 800 and 825 °C for 6 h, the density increases to 2.7386 g.cm^{-3} and 2.7482 g.cm^{-3}, respectively, due to crystallization of $ZrTiO_4$ having a theoretical density of 5.05 g.cm^{-3} [31]. After heat-treatments at 850 and 875 °C for 6 h, the density increases to 2.7890 g.cm^{-3} and then, to 2.8227 g.cm^{-3} due to additional crystalllization of the magnesium aluminosilicate glass matrix with formation of Mg-petalite and a small fraction of spinel. After the heat-treatment at 900 °C, the density of the multiphase glass-ceramic containing $ZrTiO_4$, spinel, a small fraction of Mg-petalite nanocrystals, and residual glass, close to silica glass composition, reaches the maximum value of 2.8416 g.cm^{-3}. The density decreases to the value of 2.8110 g.cm^{-3} after the heat-treatment at 950 °C. The phase assemblage of this glass-ceramic includes $ZrTiO_4$, spinel, and the residual glass phase with composition approaching silica glass. The obtained dependence of density on the heat-treatment temperature can be assigned to a complex phase assemblage of these glass-ceramics and a complex character of intergranular interaction of these phases. During the heat-treatment at 950 °C, simultaneously with crystallization of dense spinel (ρ~3.58 g.cm^{-3} [32]) and $ZrTiO_4$ (ρ~5.05 g.cm^{-3}), a light residual glass with composition close to silica is formed. Note that density of the silica glass is ~2.201 g.cm^{-3}. We can suggest that appearence of small volumes of dense phases and a large volume of the light phase leads to a decrease in the density of glass-ceramics. It is interesting that a similar density variation with the heat-treatment schedule was also found for the samples obtained by two-stage heat-treatments (Fig. 12b), which have a partly different phase assemblage. Previously, we observed similar dependences of density in magnesium aluminosilicate glass-ceramics with different spinel phase compositions obtained by two-stage heat-treatments [19], [33].The density of the glass-ceramics heat-treated at 850 °C for 24 hours is 2.8098 g.cm^{-3}, which is higher than the density of a glass-ceramic prepared at the same temperature for 6 h, probably due to a denser structure of the material (Fig. 11d), and a higher spinel crystallinity fraction.

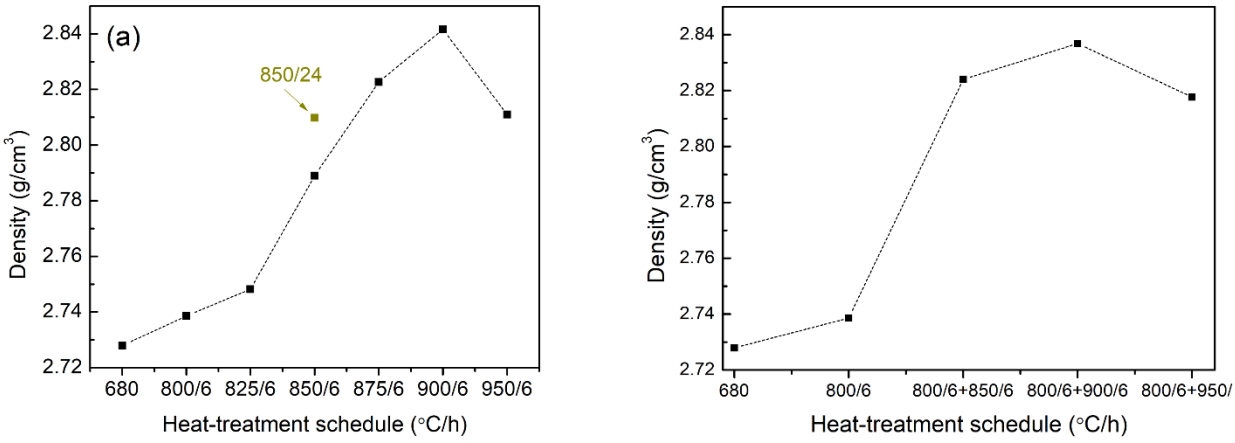

Figure 12. *Dependences of densities of the samples after single-stage (a) and two-stage (b) heat-treatments. The lines are guides for an eye. The error bars match the size of symbols.*

3.6 Optical absorption spectroscopy

Fig. 13 shows the absorption spectra of the glass and glass-ceramics. The UV absorption edge in the spectrum of the initial glass is observed at ~362 nm. The spectrum also exhibits a weak, broad band between 750-1500 nm with a maximum at ~1090 nm and a tail spanning to 2500 nm, as well as an asymmetric band between 2700-3300 nm. The spectrum bears strong similarities to the absorption spectrum of glass of the same composition nucleated solely by TiO_2 [19]. The absorption edge and absorption in the visible spectral range, up to 500 nm, is caused by various color centers giving rise to absorption bands of different origins. These include oxygen-metal charge transfer (OMCT) bands caused by $O–Ti^{3+}$ (at ~240 nm [34]), $O–Ti^{4+}$ (at ~300 nm [34]), $O–Fe^{2+}$ (at ~235 nm) and $O–Fe^{3+}$ (at ~270 nm), overlapping with bands located at longer wavelengths. These bands from 480 to 625 nm correspond to the $^2T_{2g} \rightarrow E_g$ transition of Ti^{3+} ion in the ligand field (LF) in octahedral symmetry (O_h) [35], [36]. Additional bands with maxima at 370, 380, 420, 440, and 480 nm are assigned to d-d transitions of Fe^{3+} ions in different coordination sites [37], while the peaks located at 430 and 465 nm are attributed to spin-forbidden transitions of Fe^{2+} ions, $^5T_2(D) \rightarrow {}^3T_1(H)$ and $^5T_2(D) \rightarrow {}^3T_2(H)$, respectively [37]. The peak at ~ 450 nm is due to Fe^{2+}-Ti^{4+} heteronuclear intervalence charge transfer (IVCT) [36] and the one at ~ 480 nm is due to Ti^{4+}/Ti^{3+} homonuclear IVCT [38]. The broad absorption band at 750–1500 nm with a peak at ~1090 nm can be assigned to the spin-allowed $^5T_2 \rightarrow {}^5E$ electronic d–d transition of Fe^{2+} ions in O_h site in the glass matrix [36], while a smaller fraction of Fe^{2+} ions in tetrahedral (T_d) sites (the $^5E \rightarrow {}^5T_2$ transition) is responsible for a weak absorption tail spanning up to 2500 nm [39]. The asymmetric absorption band between 2700-3100 nm is assigned to vibrations of hydroxyl groups in the initial glass [19].

The spectra of the samples heat-treated at 800 and 825 °C for 6 h are similar to each other and differ from that of the initial glass primarily by a decrease in absorption in the UV and visible (380 – 500 nm) ranges. The shift of the absorption edge from 362 to 355 and 350 nm, respectively, and the decrease in absorption in the visible range are mainly due to the decreased concentration of titanium ions in various oxidation states due to the crystallization of $ZrTiO_4$. Absorption in the IR range does not change, which means that Fe^{2+} ions do not participate in the crystallization of $ZrTiO_4$ and remain in the glass matrix.

As the heat-treatment temperature increases to 850 °C, the absorption spectrum changes significantly. There is a raise of absorption in the visible spectral range, a shift of the maximum of the absorption band of Fe^{2+} ions in O_h sites from ~1090 to ~1170 nm, an appearance of a broad band at 1400–2500 nm with a maximum at ~1850 nm due to Fe^{2+} ions in T_d sites, and a broadening of the absorption band assigned to OH- groups.

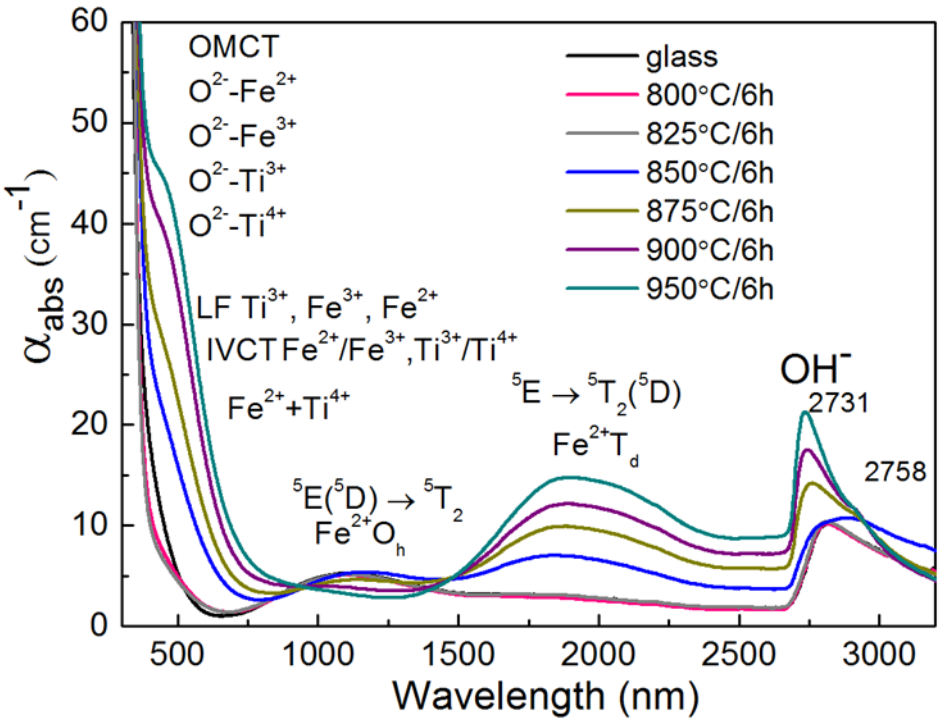

Figure 13. *Optical absorption spectra of the initial and heat-treated glass.*

These spectral changes should be caused by crystallization of Mg-petalite and spinel (Fig. 3a). It is known that petalite incorporate only small concentrations of Fe^{3+} ions in the Al^{3+} positions (0.003 Fe^{3+} per 20 oxygen atoms), which is a characteristic of aluminosilicates where all Al^{3+} ions are in tetrahedral (AlO_4) coordination [4], which may also apply for Mg-petalite. The absorption band observed in petalite at ~1170 nm is assigned to Fe^{2+} ions in O_h sites [40]. In the natural petalite structure, Li^+ ions in fourfold coordination are located between the layers of SiO_4/AlO_4 tetrahedra. According to Reisfeld *et al.* [41], in the structure of Mg-petalite, Mg^{2+} ions replace Li^+ ions and, since Mg^{2+} prefers octahedral coordination, the Mg-petalite structure may be very distorted compared to natural petalite [41]. We believe this structural distortion allows the incorporation of a small fraction of Fe^{2+} ions into Mg-petalite at Mg^{2+} positions. Therefore, we may conclude that the shift of the absorption band of octahedrally coordinated Fe^{2+} ions from ~1090 to ~1170 nm is connected to Fe^{2+} ions migrating from the glass matrix into Mg-petalite nanocrystals, occupying Mg^{2+} sites. The increase in absorption at ~1850 nm can be assigned to Fe^{2+} ions in T_d sites in spinel nanocrystals as ferrous ions replace Mg^{2+} in T_d sites [19]. The raise of absorption in the visible spectral range can be caused by electronic *d-d* transitions of $^{[4]}Fe^{2+}$ and $^{[6]}Fe^{3+}$ ions, as well as Ti^{3+} ions and the exchange-coupled pairs of these ions in the spinel nanocrystals [42], [43], in Mg-petalite and in the residual glass. The broadening of the absorption band in the range of 2650-3200 nm can be assigned to OH-groups in Mg-petalite [4].

A further increase in the temperature of a single-stage heat-treatment causes gradual changes in the absorption spectra: absorption in the visible region increases; absorption of octahedrally coordinated Fe^{2+} ions centered around 1090 nm decreases and eventually disappears; absorption centered around ~1850 nm due to Fe^{2+} ions in T_d sites increases; the absorption band of OH-groups narrows and its maximum shifts to shorter wavelengths. These spectral changes originate from the gradual diminishing and then disappearance of Mg-petalite and gradual growth of spinel crystal fraction. The increase of absorption intensity in the visible region, despite the disappearance of Mg-petalite from the glass-ceramics assemblage (Fig. 3a), indicates that the main contribution to this absorption are iron ions in spinel nanocrystals, with a smaller contribution from those in the residual glass. The increase in the intensity of the absorption band at ~1850 nm is caused by the increasing fraction of spinel crystal-

lites doped with $^{[4]}Fe^{2+}$ ions as the heat-treatment temperature rises up to 950 °C. The transformation of the shape of the absorption band connected with hydroxyl groups caused by spinel crystallization is discussed elsewhere [19].

This type of spectrum is very similar to that obtained by the two-stage heat-treatment with a second-stage temperature of 950 °C (Fig. 14a), which is in accordance with the comparable phase compositions of glass-ceramics obtained by single- and two-stage heat-treatments (Fig. 3a,b, Fig. 10, and Table 1 for comparison).

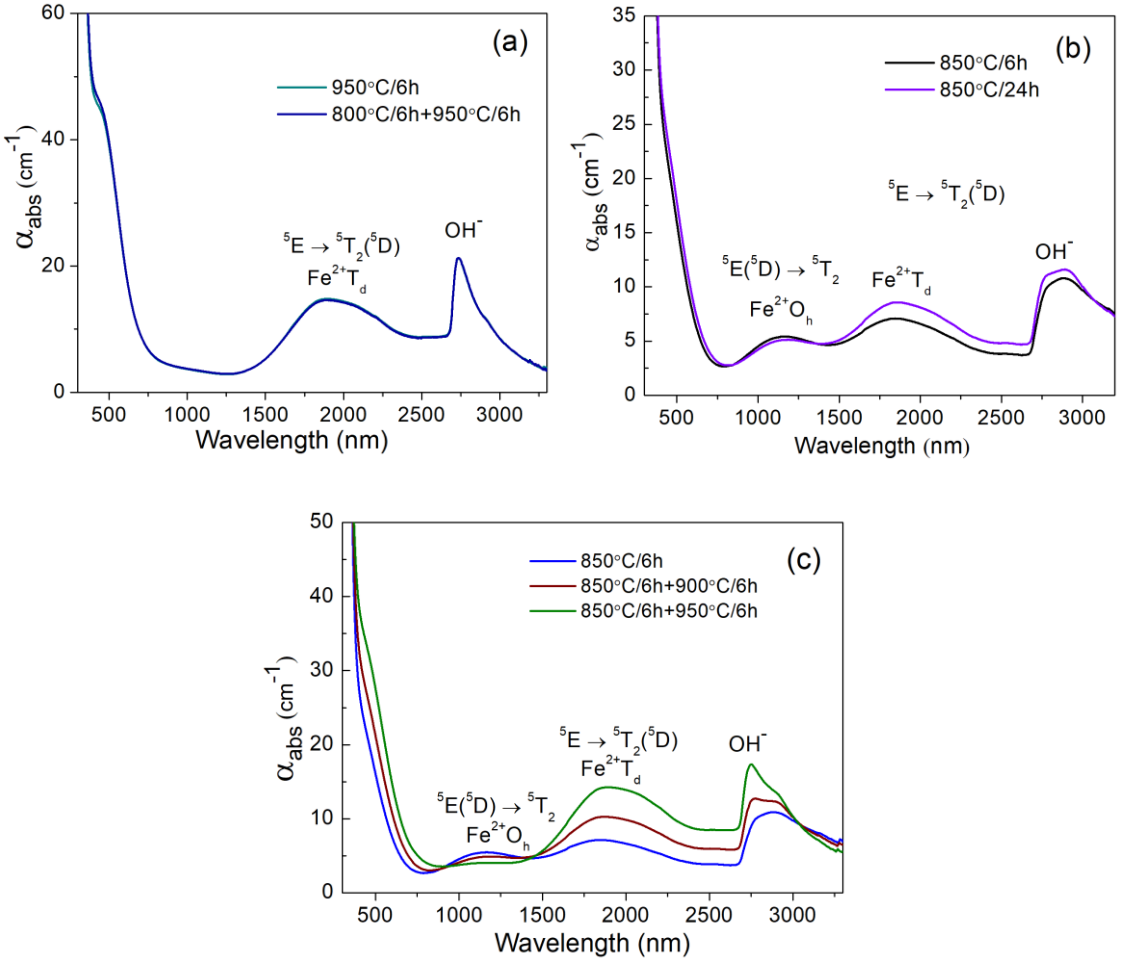

Figure 14. *Optical absorption spectra of glass-ceramics obtained by (a) heat-treatments at 950 °C using single- and two-stage schedules; (b) heat-treatments at 850 °C for 6 and 24 h; (c) the single-stage heat-treatment at 850 °C and two-stage heat-heat-treatments with the first hold at 850 °C. Labels indicate the heat-treatment schedules.*

Fig. 14b shows the absorption spectra of transparent glass-ceramics obtained by heat-treatments at 850 °C for 6 and 24 h. They are similar and exhibit broad unstructured bands centered at 1170 and 1860 nm, and an absorption band of OH- groups in the range of 2700-3300 nm. Increasing the heat-treatment time from 6 to 24 h results in an increase of the band at 1860 nm associated with $^{[4]}Fe^{2+}$ ions in spinel nanocrystals probably at the expense of $^{[6]}Fe^{2+}$ ions in Mg-petalite. Note that the intensity is expected to increase by an order of magnitude in going from O_h to T_d sites, as T_d sites lack a center of inversion symmetry. Therefore, even a negligible decrease of intensity assigned to absorption of $^{[6]}Fe^{2+}$ species can lead to a noticeable increase of intensity assigned to absorption of $^{[4]}Fe^{2+}$ species.

Fig. 14c presents the absorption spectra of glass-ceramics obtained by single-stage heat-treatment at 850 °C and two-stage heat-treatments with the first hold at 850 °C and the second

hold at 900 °C or 950 °C. The second-stage heat-treatments cause a decrease in the intensity of the absorption band characteristic of iron-containing Mg-petalite at ~1170 nm, an increase in absorption in the visible range and around 1900 nm, as well as a structuring of the hydroxyl band. These changes are due to the evolution in the phase composition of the samples shown in Fig. 5a, specifically a decrease in the fraction of Mg-petalite and an increase in the fraction of spinel. Therefore, the absorption at ~1900 nm, attributed to $^{[4]}Fe^{2+}$ ions in spinel nanocrystals, can be used as a spectral indicator of spinel formation.

3.7 Linear coefficients of thermal expansion

The thermal expansion coefficients of the initial and heat-treated glasses in the temperature range from 20 to 320 °C are listed in Table 4. The initial glass has a thermal expansion coefficient of ~3.4×10^{-6} K^{-1}. The glass heat-treated at the nucleation stage of 800 °C for 6 h has the thermal expansion coefficient slightly increased to 3.6×10^{-6} K^{-1}. The glass-ceramic with Mg-petalite as the main crystalline phase obtained by heat-treatment at 850 °C for 6 h has thermal expansion coefficient of ~4.4×10^{-6} K^{-1}. In spite of quite different phase assemblages in glass-ceramics prepared at 850 °C for 6 h by single- and two-stage heat-treatments, their expansion coefficients are nearly identical (Table 5). As a rule, the diversity of amorphous and crystalline phases in the phase assemblage of glass-ceramics is responsible for their thermal expansion.

Table 4. *The thermal expansion coefficients (CTE) in the temperature range from 20 to 320 °C for the initial and heat-treated glass.*

Heat-treatment schedule	**CTE_{20-320} ($\times10^{-6}$ K^{-1})**	**Phase assemblage**
Initial glass	3.43 ± 0.07	-
800 °C for 6 h	3.61 ± 0.07	$ZrTiO_4$
850°C for 6 h	4.44 ± 0.09	$ZrTiO_4$, Mg-petalite, spinel (traces)
800 °C, 6 h+850 °C, 6 h	4.43 ± 0.09	$ZrTiO_4$, Mg-petalite (traces), spinel

However, in the sample that underwent single-stage heat-treatment at 850 °C, Mg-petalite is the dominant phase and therefore it can be assumed that the thermal expansion coefficient of ~4.4×10^{-6} K^{-1} is largely due to the appearance of this phase.

4. Discussion

The initial glass is X-ray amorphous. The liquid-liquid phase separated structure, confirmed by its SEM image (Fig. 11a), is developed in the course of melt casting and cooling. The observed development of the structural inhomogeneity upon heat-treatment of the glass at the nucleation stage (800 °C for 6 h) can be associated with both the phase separation (changes in the composition and volume of phase-separated regions) and the crystallization of $ZrTiO_4$. Following Barry *et al.* [14] and Fernandez-Martin *et al.* [44], we may suggest that some proportions of MgO and Al_2O_3 entered these regions together with TiO_2 and ZrO_2. A small portion of spinel solid solution can be formed within these regions at elevated temperatures, accompanying the crystallization of Mg-petalite, which occurs from the residual magnesium aluminosilicate glass.

4.1 Crystallization of Mg-petalite

As we mentioned above, in the DSC curves of the quenched glass obtained at heating rates of 5 and 10 $K\cdot min^{-1}$, the exothermic peaks appear only due to the crystallization of $ZrTiO_4$ and spinel. No exothermic peak can be assigned to Mg-petalite. Nevertheless, Mg-petalite crystallizes in glass-ceramics accompanied by $ZrTiO_4$ and spinel. Mg-petalite is the predominant phase in glass-ceramics obtained by single-stage heat-treatments at 850 °C for 3 to 24 h and at 875 °C for 6 h. As a result of its crystallization, the amorphous halo disappears from the XRD pattern implying a high degree of crystallization. The amorphous halo appears as traces

in glass-ceramic prepared at 900 °C for 6 h (Fig. 3a). Traces of Mg-petalite are also found in glass-ceramics obtained by the two-stage heat-treatment with the first hold at 800 °C for 6 h and the second hold at 850 °C for 6 h (Fig. 3b).

The study of the phase composition of glass-ceramics obtained by heat-treatments at 850 °C from 0 to 24 h (Fig. 4), revealed that only $ZrTiO_4$ crystallizes during the temperature raise from room temperature to 850 °C, with its fraction being much smaller than in samples obtained by heat-treatments at 800 and 825 °C for 6 h (Fig. 15). The formation of Mg-petalite begins after 3 h of holding. Therefore, the absence of the exothermic event on the DSC curve assigned to Mg-petalite can be explained by the slow rate of its crystallization from the magnesium aluminosilicate base glass. We may speculate that the heat-treatment time necessary to activate diffusion and ordering required for the formation of complex aluminosilicate chains in a highly viscous magnesium aluminosilicate glass would be too long for the crystallization of Mg-petalite to occur during the DSC heating ramp.

4.2 Crystallization of spinel

The mechanism of spinel crystallization upon two-stage heat-treatments has been investigated by Golubkov *et al.* [22] for a magnesium aluminosilicate glass with the same composition as the present one, nucleated by 10 mol% TiO_2. It was demonstrated using the small-angle X-ray scattering findings [22] that the initial glass had an inhomogeneous structure, which was formed by a spinodal decomposition mechanism. This inhomogeneity ensured the regular distribution of the crystalline phases that appeared during further heat-treatments. Spinel was the second phase to crystalize from smaller inhomogeneous regions at elevated temperatures, after crystallization of magnesium aluminotitanate solid solutions from larger inhomogeneous regions at lower temperatures. We suggested that different crystallization rates of these phases were originated by different mobilities of their structural units [12]. We believe a similar mechanism is responsible for the spinel crystallization in the glass under study, nucleated by a mixture of TiO_2 and ZrO_2.

From the DSC curves of the quenched glass and the glass heat-treated at 800 °C (Fig. 6), it is seen that they only differ in the absence of the crystallization peak of $ZrTiO_4$ in the sample heat-treated at 800 °C, since zirconium titanate has already crystallized in this sample [20]. Thus, holding at the nucleation stage of 800 °C is not required for the spinel crystallization, which occurs at a higher temperature, $T_{on\ spinel}$ = 925 °C (Fig. 2). To confirm this assumption, we heated the initial glass up to 850, 900, and 950 °C and the samples were quenched from the furnace to cool in air. Their XRD patterns are shown in Fig. 15 in comparison with those of the glass and samples subjected to single-stage heat-treatments at 800 °C or 825 °C for 6 h. In accordance with the DSC curve of the initial glass, only $ZrTiO_4$ crystallizes in glass heated up to 900 °C, which does not influence the composition of the residual glass, as the position of the amorphous halo remains unchanged in the XRD pattern. Spinel crystallization takes place when the temperature is raised from 900 to 950 °C, which leads to a pronounced shift of the amorphous halo to the position characteristic of silica glass (Fig. 3a). Holding at 950 °C is not required to develop the spinel growth process.

4.3 Competing crystallization mechanisms

Two competing phase transformation processes are developed during the second stage of the two-stage heat-treatment when the second hold temperature is 850 °C. They are spinel crystallization, which depletes the residual glass of Mg and Al ions, as indicated by the displacement of the amorphous halo to 2θ=23.0 °, and the crystallization of trace amounts of Mg-petalite. The same processes occur at the single-stage holding at 900 °C.

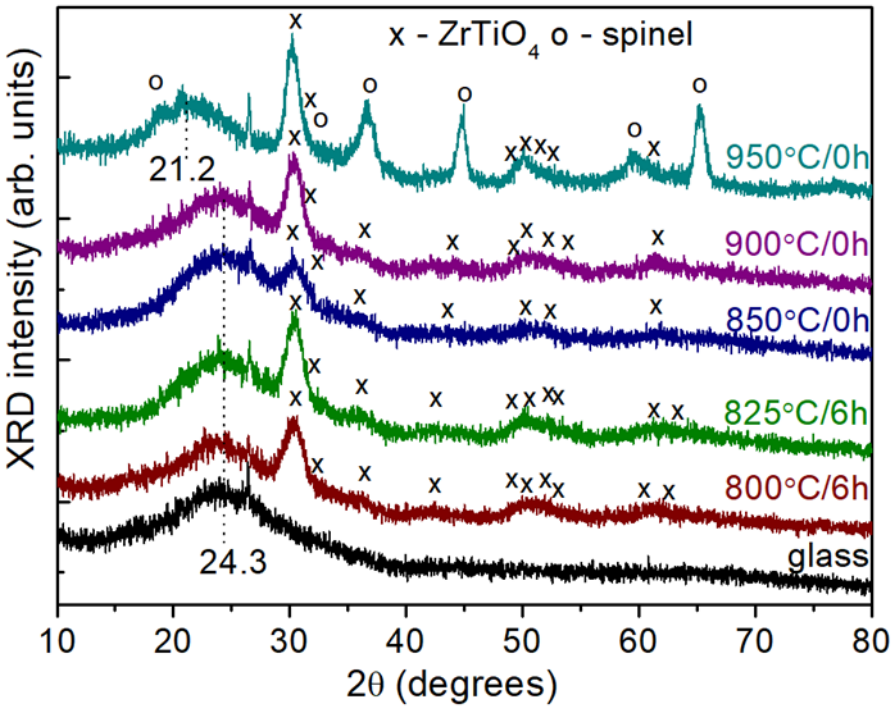

Figure 15. *XRD patterns of the initial and heat-treated glass. The dashed lines show the position of the maximum of the amorphous halo. The patterns are shifted for better observation.*

We may speculate that the temperature increase to 850 °C without isothermal holding at this temperature does not allow the formation of a well-developed liquid-liquid phase-separated structure similar to the one formed during the nucleation heat-treatment at 800 °C for 6 hours. At this temperature rise, only a small fraction of $ZrTiO_4$ crystallizes (Fig. 15). During holding at 850 °C, there are two competing processes. The spinel crystallization is hindered by the undeveloped liquid-liquid phase separation, and the competing process of the Mg-petalite crystallization from the residual glass dominates. As a result of this process, the amorphous halo disappears.

We may suggest that raising the temperature to 900 °C without isothermal holding allows the formation of the developed liquid-liquid phase-separated structure similar to that formed during the nucleation heat-treatment at 800 °C for 6 hours. Holding at 900 °C for 6 h leads to the same phase assemblage as the two-stage heat-treatment at 800 °C, 6 h + 850 °C, 6 h (Figs 3a,b). However, the spinel crystallization is more pronounced, as the spinel crystallinity fraction is larger, the Mg-petalite fraction is smaller and the position of the amorphous halo is shifted to 2θ=21.3 °.

The temperature rise to 950 °C causes the development of liquid-liquid phase separation and spinel crystallization, so that the residual glass becomes highly siliceous. Crystallization of Mg-petalite from such residual glass is impossible.

Let us discuss the influence of the first-stage heat-treatment and its temperature on the phase assemblage of glass-ceramics (Figs 16-21). As we mentioned above, the heat-treatment at the nucleation stage (800 °C for 6 h) leads not only to the crystallization of $ZrTiO_4$ but also to the development of a rich liquid-liquid phase-separated structure (Fig. 11b), which seems to be an important step in the formation of transparent spinel-based glass-ceramic. Heating even at the temperature of 850 °C at the second stage, results only in traces of Mg-petalite in addition to $ZrTiO_4$ and spinel nanocrystals (Fig. 16). The $ZrTiO_4$, Mg-petalite and spinel crystallized by the two-stage heat-treatment have smaller sizes (6.0, 16.0 and 8.5 nm, respectively), as compared with those obtained from the single-stage heat-treatment at 850 °C (6.2, 29 and 9.5 nm, respectively). Two competing phase transformation processes take place

and influence the crystallization kinetics of the two phases and the composition of the residual glass. The amorphous halo in the XRD pattern of the glass-ceramic obtained by the two-stage heat-treatment at 800 °C for 6 h + 850 °C for 6 h is located at 2θ=23.0 °, which is evidence of incomplete spinel crystallization. In the absorption spectrum of the sample obtained by the two-stage heat-treatment (Fig. 17), there is a near disappearance of the absorption band of

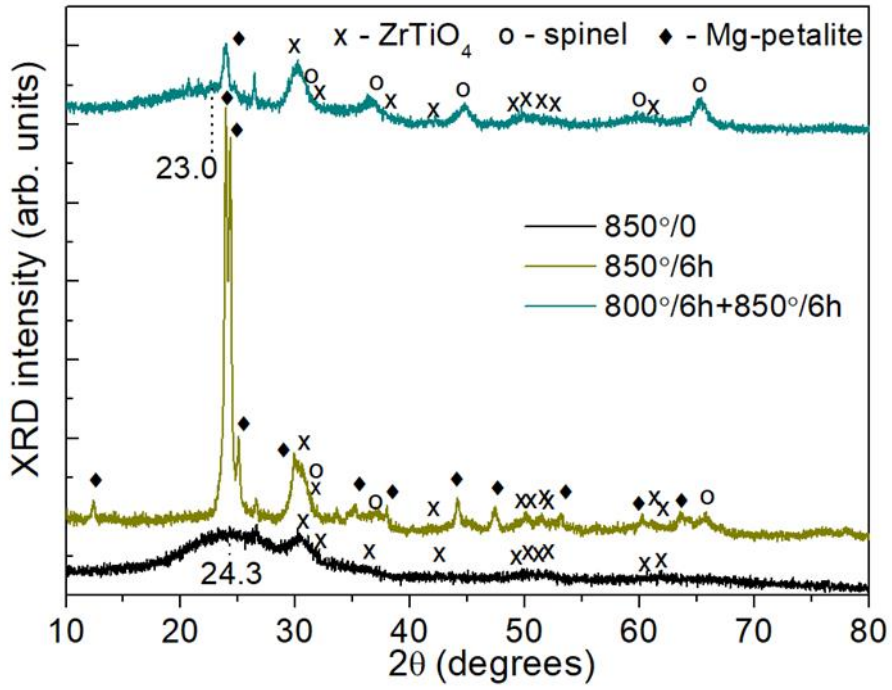

Figure 16. *XRD patterns of glass-ceramics obtained at 850 °C by single- and two-stage heat-treatments. Labels indicate heat-treatment schedules. The dashed line shows position of the maximum of the amorphous halo. The patterns are shifted for better observation.*

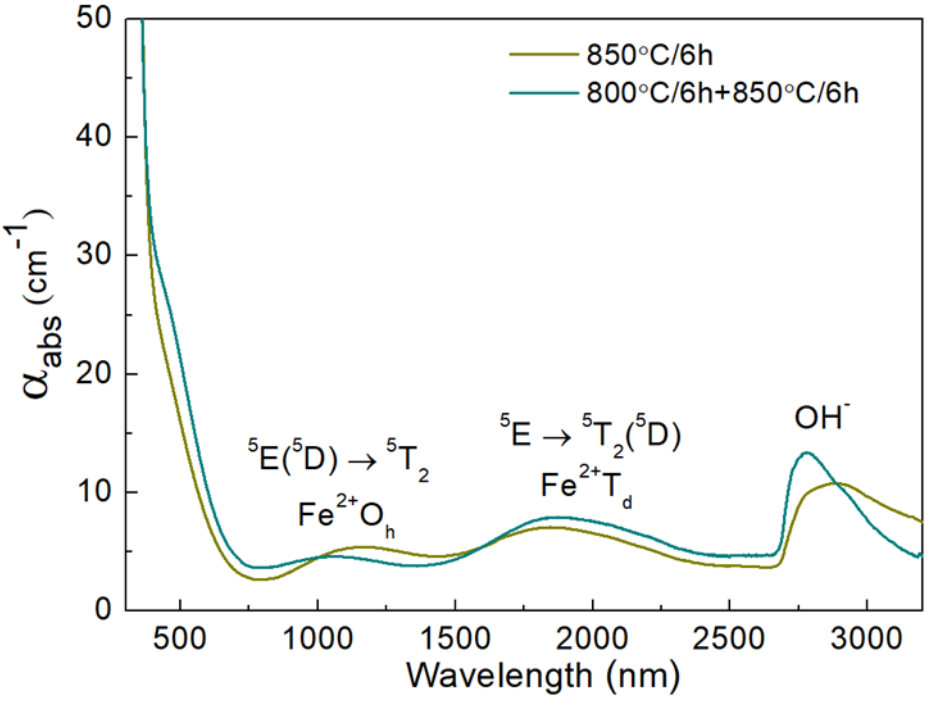

Figure 17. *Optical absorption spectra of glass-ceramics obtained at 850 °C by single- and two-stage heat-treatments.*

$^{[6]}Fe^{2+}$ ions in Mg-petalite nanocrystals and an increase in the absorption band due to $^{[4]}Fe^{2+}$ ions in spinel nanocrystals, compared to the absorption spectrum of the sample obtained by the single-stage heat-treatment at 850 °C for 6 h. This change is explained by the difference in their phase assemblages.

XRD patterns of glass-ceramics obtained at 900 °C by single- and two-stage heat-treatments show the strong impact of the two-stage heat–treatment on the phase composition of glass-ceramics (Fig. 18). Raising the temperature to 900 °C without isothermal holding allows the formation of well-developed liquid-liquid phase-separated structure similar to that formed during the nucleation heat-treatment at 800 °C for 6 hours, with the crystallization of $ZrTiO_4$ with a mean size of 5.8 nm. Holding at 900 °C for 6 h leads to the same phase assemblage as the two-stage heat-treatment at 800 °C, 6 h + 850 °C, 6 h with somewhat more developed spinel crystallization, as the spinel crystallinity fraction is larger, the Mg-petalite fraction is smaller and the position of the amorphous halo is shifted to 2θ=21.3 °. After two-stage heat-treatment with the first hold at 800 °C for 6 hours, Mg-petalite is not found. The mean sizes of the $ZrTiO_4$ and spinel crystallites are 6.5 and 9.5 nm, respectively, and are very similar to those in glass-ceramic obtained by the single-stage heat-treatment at 900 °C (Table 1). Similar phase assemblages of these glass-ceramics are responsible for the similarity of their optical absorption spectra (Fig. 19).

Mg-petalite crystallized during the heat-treatment at 850 °C for 6 h is preserved during the second-stage heat-treatment at 900 °C for 6 h, which is accompanied by $ZrTiO_4$ and spinel crystalline phases. The spectral features of Fe^{2+}-doped Mg-petalite and spinel are clearly seen in the absorption spectrum of the glass-ceramic (Fig. 19). The smaller spinel crystallinity fraction is revealed by a lower absorption intensity of the peak at ~1900 nm due to $^{[4]}Fe^{2+}$ ions in spinel nanocrystals.

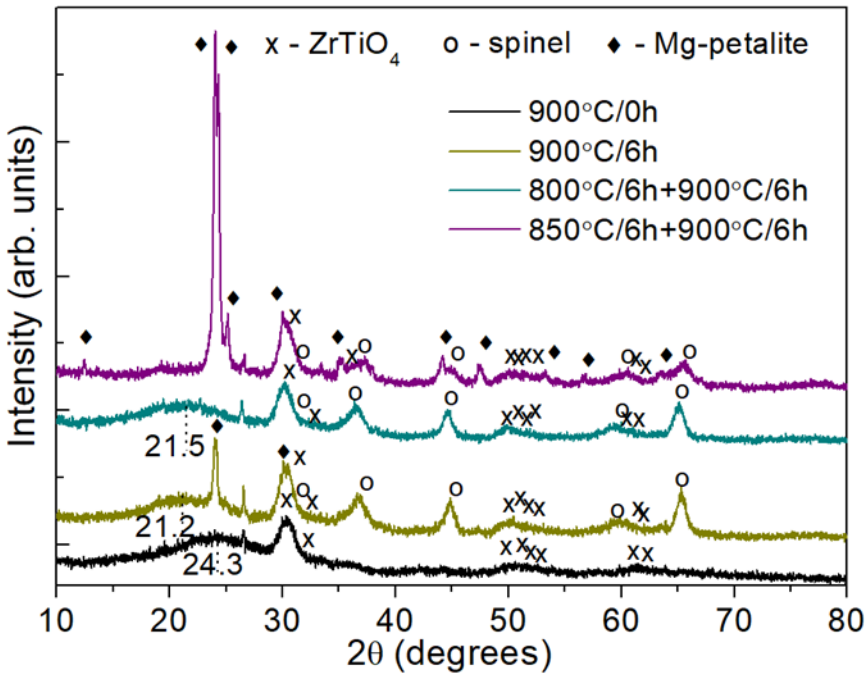

Figure 18. *XRD patterns of glass-ceramics obtained at 900 °C by single- and two-stage heat-treatments. Labels indicate heat-treatment schedules. The dashed lines show the position of the maximum of the amorphous halo. The patterns are shifted for better observation.*

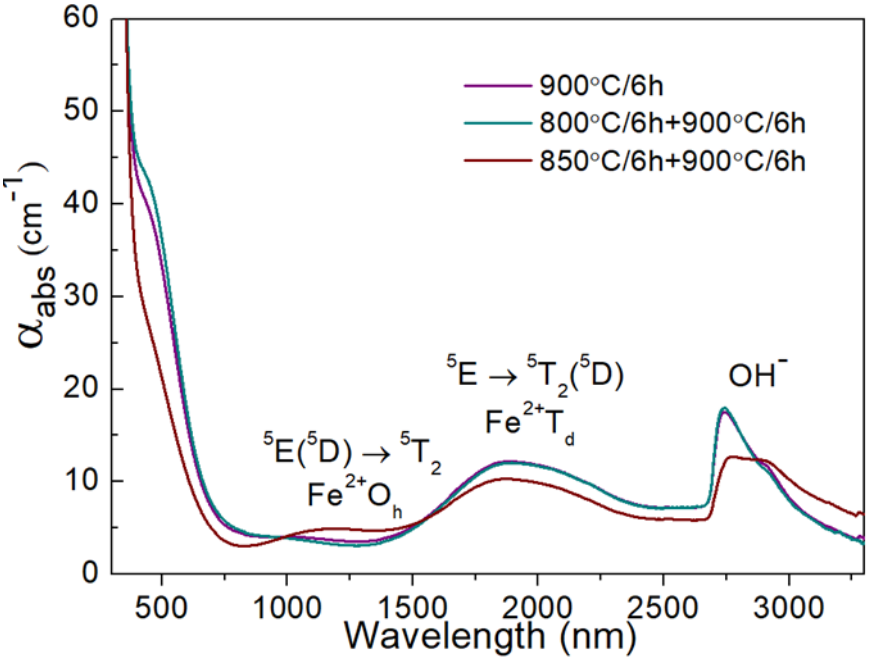

Figure 19. *Absorption spectra of glass-ceramics obtained at 900 °C by single- and two-stage heat-treatments.*

As mentioned above, the temperature rise to 950 °C causes the development of liquid-liquid phase separation and spinel crystallization, so that the residual glass becomes highly siliceous (see the position of the amorphous halo in Fig. 20). Crystallization of Mg-petalite from such glass is impossible as it is depleted of magnesium and aluminum cations. It is not surprising that glass-ceramics obtained by a simple heating to 950 °C, during the single-stage heat-treatment at 950 °C for 6 h and during two-stage heat-treatments at 800 °C, 6 h+950 °C, 6 h have similar phase compositions. They contain $ZrTiO_4$ nanocrystals with mean sizes of 6.5-8.0 nm and spinel nanocrystals with mean sizes of 9-12 nm located in the highly siliceous

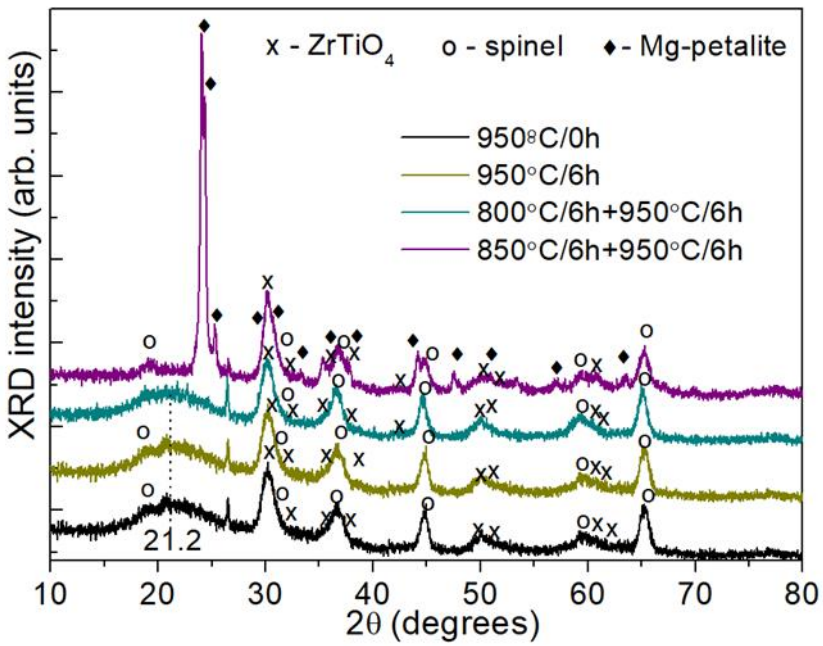

Figure 20. *XRD patterns of glass-ceramics obtained at 950 °C by single- and two-stage heat-treatments. Labels indicate heat-treatment schedules. The dashed lines show the position of the maximum of the amorphous halo. The patterns are shifted for better observation.*

residual glass with the similar position of the amorphous halo 2θ=21.2 °. The similarity of the phase compositions is reflected in similar absorption spectra (Fig. 21).

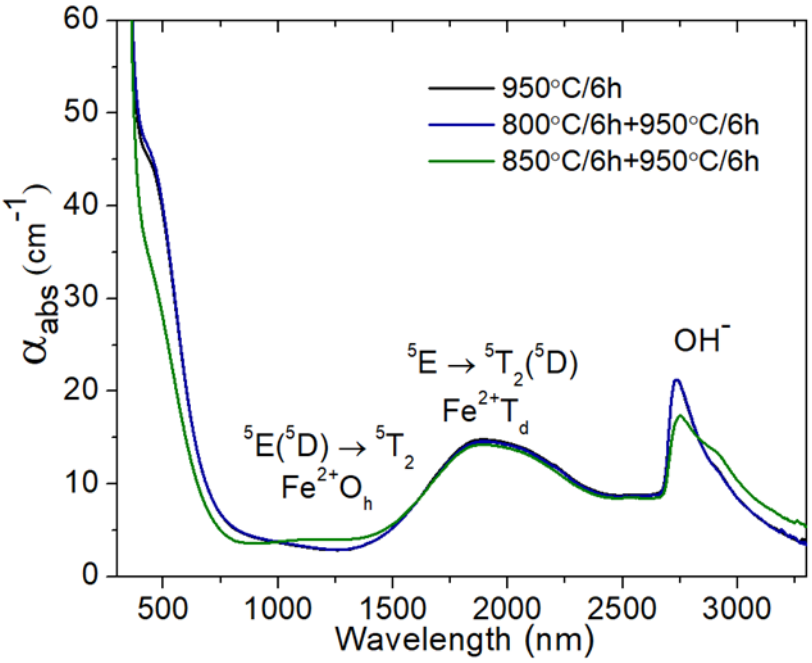

Figure 21. *Optical absorption spectra of glass-ceramics obtained at 950 °C by single- and two-stage heat-treatments.*

The glass-ceramic prepared by the two-stage heat-treatment at 850 °C for 6 h+950 °C for 6 h contains Mg-petalite, spinel and $ZrTiO_4$ with mean sizes of 29.2, 9.5 and 7.5 nm, respectively (Fig. 20 and Table 1). It is interesting that its optical absorption spectrum in the range of 1600 – 2400 nm is similar to the one of other glass-ceramics obtained by heat-treatment at 950 °C (Fig. 21). Using the absorption of $^{[4]}Fe^{2+}$ ions in spinel nanocrystals as a spectral probe of spinel formation, we may conclude that spinel crystallinity fraction at 950 °C is determined not by the thermal prehistory of glass-ceramics but by the temperature of the high-temperature heat-treatment.

5. Conclusions

Transparent glass-ceramics of the magnesium aluminosilicate system, nucleated by TiO_2 and ZrO_2, and based on Fe^{2+}:Mg-petalite and/or Fe^{2+}:$MgAl_2O_4$ spinel nanocrystals, were developed by single- and two-stage heat-treatment schedules in the temperature range from 800 to 1000 °C. The initial glass is X-ray amorphous and structurally inhomogeneous. Its absorption in the visible spectral range is caused by iron and titanium ions and their interactions, while the broad absorption band at 750–1500 nm with a peak at ~1090 nm is assigned to the spin-allowed electronic d–d transition of Fe^{2+} ions in O_h sites in the glass matrix.

Nanocrystals of $ZrTiO_4$ with mean size of ~6 nm are formed upon heating the glass up to 850 °C and during isothermal heat-treatments at 800 and 825 °C for 6 h. Fe^{2+} ions remain in the glass matrix during crystallization of $ZrTiO_4$.

Mg-petalite crystallites, ~30 nm in size, appear as the predominant phase during single-stage heat-treatments in the narrow temperature range of 850-875 °C for 3 h and above, accompanied by the crystallization of $ZrTiO_4$ and traces of spinel. During the process, Fe^{2+} ions enter the O_h sites (in Mg^{2+} positions) in Mg-petalite and the T_d sites (in Mg^{2+} positions) in spinel nanocrystals. Once formed, Mg-petalite is preserved in glass-ceramics heat-treated up to 1000 °C.

Spinel nanocrystals, ranging from 9-14 nm in size, are formed during two-stage heat-treatments with the first stage at 800 °C and the second stage from 850 to 1000 °C, during single-stage heat-treatments from 900 to 1000 °C and at a simple heating to 950 - 1000 °C. The optical absorption spectra of the spinel-based glass-ceramics develop characteristic band at around ~1900 nm due to $^{[4]}Fe^{2+}$ ions in spinel nanocrystals. This absorption can be used as a spectral indicator of spinel formation.

The heat-treatment at the nucleation stage of 800 °C for 6 h, which leads not only to crystallization of $ZrTiO_4$ but also to the development of the rich liquid-liquid phase-separated structure, seems to be an important step in the formation of transparent spinel-based glass-ceramic in a wide temperature range.

Competing crystallization mechanisms are studied. Spinel crystallizes in conditions where the developed liquid-liquid phase-separated structure is present. This crystallization is accompanied by the formation of a high-siliceous glass, from which the crystallization of Mg-petalite is inhibited. In materials with weakly developed liquid-liquid phase-separated structure, crystallization of Mg-petalite from the magnesium aluminosilicate glass predominates, and spinel crystallizes as an additional phase probably from inhomogeneous regions enriched with Ti, Zr, Mg and Al cations.

The glass-ceramics exhibit intense absorption in the spectral range of 1.6-2.4 μm due to Fe^{2+} ions in T_d sites in spinel nanocrystals, which is important for the development of saturable absorbers in this spectral range.

Data availability statement

The data presented in this study are available within the article. Additional data are available from the corresponding author upon request.

Author contributions

Vasilisa Bukina: Investigation, Writing –Original Draft. Olga Dymshits: Conceptualization, Funding acquisition, Investigation, Methodology, Supervision, Writing –Original Draft, Writing – review & editing. Irina Alekseeva: Investigation, Methodology. Anna Volokitina: Investigation. Maxim Tenevich: Investigation. Anastasia Bachina: Investigation, Writing –Original Draft. Aleksandr Zhilin: Writing – review & editing.

Competing interests

The authors declare that they have no competing interests.

Acknowledgement

The SEM study was performed using the analytical equipment of the Engineering Center of the St. Petersburg State Institute of Technology. We also thank L. Cormier for his valuable comments.

References

[1] J. B. d'Andrada, "Description of some new fossils," (Old English translation), A Journal of Natural Philosophy, Chemistry, and the Arts, vol. 5, pp. 211-213, 1801.

[2] A. Zemann-Hedlik, and J. Zemann, "Die Kristallstruktur von Petalit, $LiAlSi_4O_{10}$," Acta Cryst., vol. 8, pp. 781–787, 1955, doi: 10.1107/S0365110X55002405.

[3] F. Liebau, “Structural Chemistry of Silicates – Structure, Bonding and Classification,” Berlin, Heidelberg, New York, Tokyo: Springer-Verlag, 1985.
[4] P. Černý and D. London, “Crystal chemistry and stability of petalite,” TMPM Tschermaks Min. Petr. Mitt., vol. 31, pp. 81-96, 1983, doi :10.1007/BF01084763.
[5] G. H. Beall, Q. Fu, and C. M. Smith, “High strength glass-ceramics having petalite and lithium silicate structures”, U.S. Patent Application US20160102010A1, 2017.
[6] W. Schreyer and J. F. Schairer, “Metastable solid solutions with quartz-type structures on the join SiO_2 – $MgAl_2O_4$,” Z. Kristallogr. Krist., vol. 116, pp. 60-82, 1961, doi: 10.1524/zkri.1961.116.16.60.
[7] W. Schreyer and J. F. Schairer; “Metastable osumilite- and petalite-type phases in the system MgO-Al_2O_3-SiO_2,” Amer. Mineral., vol. 47 (1-2), pp. 90–104, 1962.
[8] S. B. Holmquist, “A note on a “Mg petalite″ phase”, Z. Kristallogr. Krist., vol. 118, (1-6) pp. 477-478, 1963, doi: 10.1524/zkri.1963.118.16.477.
[9] M. A. Conrad, “Phase transitions in a zirconia-nucleated MgO Al_2O_3·3SiO_2 glass – ceramic,” J. Mater. Sci., vol. 7, pp. 527 – 530, 1972, doi: 10.1007/BF00761951.
[10] I. Alekseeva, O. Dymshits, V. Golubkov, A. Shashkin, M. Tsenter, A. Zhilin, and W.-B. Byun, “Phase transformations in NiO and CoO doped magnesium aluminosilicate glasses nucleated by ZrO_2,” Glass Technol., vol. 46 (2), pp. 187–191, 2005.
[11] B. G. Varshal, L. Y. Baiburt, A. M. Gelberger, N. N. Malakhovskaja, and A. P. Naumkin, “Synthesis of metastable Mg- and Zn-containing petalite-like phases,” Isv. Akad. Nauk S.S.S.R. Neorg. Mater., vol. 7 (4), pp. 712, 1971; VINITI Publ. N2482-71, 1971 (Vsesoyusnyi Institut Nauchno-Tekhnicheskoi Informatsii).
[12] L. R. Pinckney and G. H. Beall, “Nanocrystalline non-alkali glass-ceramics,” J. Non-Cryst. Solids, vol. 219, pp. 219-227, 1997, doi: 10.1016/S0022-3093(97)00272-X.
[13] A. V. Bortkevich, O. S. Dymshits, A. A. Zhilin, A. Yu. Polushkin, M. Ya. Tsenter, A. V Shashkin, V. V. Golubkov, V. B. Ben, K. K. Li, E. B. Pak, and K. H. Pak, “Study of phase transformations in titanium-containing magnesium-aluminum silicate glasses and glass-ceramics for diffuse reflectors,” J. Opt. Technol., vol. 69 (8), pp. 588-594, 2002, https://opg.optica.org/jot/abstract.cfm?URI=jot-69-8-588.
[14] T. I. Barry, J. M. Cox, and R. Morrell, “Cordierite glass-ceramics - effect of TiO_2 and ZrO_2 content on phase sequence during heat treatment,” J. Mater. Sci., vol. 13, pp. 594–610, 1978, doi:10.1007/BF00541810.
[15] A. Buch, M. Ish-Shalom, R. Reisfeld, A. Kisilev, and E. Greenberg, “Transparent glass ceramics: Preparation, characterization and properties,” Mater. Sci. Eng., vol. 71, pp. 383-389, 1985, doi: 10.1016/0025-5416(85)90257-5.
[16] U. Lembke, R. Brückner, R. Kranold, and T. Höche, “Phase formation kinetics in a glass ceramic studied by small-angle scattering of X-rays and neutrons and by visible-light scattering,” J. Appl. Crystallogr., vol. 30, pp. 1056 – 1064, 1997, doi: 10.1107/S0021889897001313.
[17] G. Carl, T. Höche, and B. Voigt, “Crystallisation behavior of a MgO–Al_2O_3–SiO_2–TiO_2–ZrO_2 glass,” Phys. Chem. Glasses, vol. 43C, pp. 256–258, 2002.
[18] K. Maeda and A. Yasumori, “Effect of molybdenum and tungsten oxides on nucleation and crystallization behaviors of MgO–Al_2O_3–SiO_2 glasses,” J. Non-Cryst. Solids, vol. 427, 152-159, 2015, doi: 10.1016/j.jnoncrysol.2015.07.040.
[19] L. Basyrova, V. Bukina, S. Balabanov, A. Belyaev, V. Drobotenko, O. Dymshits, I. Alekseeva, M. Tsenter, S. Zapalova, A. Khubetsov, A. Zhilin, A. Volokitina, V. Vitkin, X. Mateos, J.M. Serres, P. Camy, and P. Loiko, “Synthesis, structure and spectroscopy of Fe^{2+}:$MgAl_2O_4$ transparent ceramics and glass-ceramics,” J. Lumin., vol. 236, pp. 118090, 2021, doi: 10.1016/j.jlumin.2021.118090.
[20] V. S. Bukina, O. S. Dymshits, I. P. Alekseeva, A. A. Volokitina, S. S. Zapalova, and A. A. Zhilin, “Optical glass-ceramics based on Fe^{2+}: $MgAl_2O_4$ nanocrystals and nucleated by TiO_2 and ZrO_2,” Nanosyst.: Phys. Chem. Math., vol. 14 (6), pp. 690–698, 2023, doi: 10.17586/2220-8054-2023-14-6-690-698.
[21] H. Lipson, H. Steeple, in: McMillan (Ed.), Interpretation of X-Ray Powder Patterns, Martins Press, London, N.Y., 1970, p. 344.

[22] V. V. Golubkov, O. S. Dymshits, A. A. Zhilin, T. I. Chuvaeva, and A. V. Shashkin, “On the phase separation and crystallization of glasses in the $MgO–Al_2O_3–SiO_2–TiO_2$ system,” Glass. Phys. Chem., vol. 29 (3), pp. 254–266, 2003.
[23] V. V. Golubkov, O. S. Dymshits, V. I. Petrov, A. V. Shashkin, M. Ya. Tsenter, A. A. Zhilin, and Kang Uk, “Small-angle X-ray scattering and low-frequency Raman scattering study of liquid phase separation and crystallization in titania-containing glasses of the $ZnO–Al_2O_3–SiO_2$ system,” J. Non-Cryst. Solids, vol. 351, pp. 711-721, 2005, doi: 10.1016/j.jnoncrysol.2005.01.071.
[24] A. Dugué, O. Dymshits, L. Cormier, P. Loiko, I. Alekseeva, M. Tsenter, K. Bogdanov, G. Lelong, and A. Zhilin, “Structural transformations and spectroscopic properties of Ni-doped magnesium aluminosilicate glass-ceramics nucleated by a mixture of TiO_2 and ZrO_2 for broadband near-IR light emission,” J. Alloys Compd., vol. 780, pp. 137-146, 2019, doi: 10.1016/j.jallcom.2018.11.247.
[25] M. A. Krebs and R. A. Condrate, “A Raman spectral characterization of various crystalline mixtures in the ZrO_2-TiO_2 and HfO_2-TiO_2 systems,” J. Mater. Sci. Lett., vol. 7, pp. 1327–1330, 1988, doi: 10.1007/BF00719973.
[26] F. Azough, R. Freer, and J. Petzelt, “A Raman spectral characterization of ceramics in the system $ZrO_2–TiO_2$,” J. Mater. Sci., vol. 28, pp. 2273–2276, 1993, doi: 10.1007/BF01151652.
[27] https://rruff.info/petalite/R060365.
[28] A. A. Kaminskii, E. Haussühl, H. J. Eichler, J. Hanuza, M. Mączka, H. Yoneda, and A. Shirakawa, “Lithium silicate, $LiAlSi_4O_{10}$ (petalite)—a novel monoclinic SRS-active crystal,” Laser Phys. Lett., vol. 12, pp. 085002(1-8), 2015, doi: 10.1088/1612-2011/12/8/085002.
[29] D. P. C. Thackeray, “The Raman spectrum of zirconium dioxide,” Spectrochim. Acta A. Mol. Biomol. Spectrosc., vol. 30, (2) pp. 549-550, 1974, doi: 10.1016/0584-8539(74)80096-6.
[30] I. Alekseeva, A. Baranov, O. Dymshits, V. Ermakov, V. Golubkov, M. Tsenter, and A. Zhilin, “Influence of CoO addition on phase separation and crystallization of glasses of the ZnO-Al_2O_3-SiO_2-TiO_2 system,” J. Non-Cryst. Solids, vol. 357, pp. 3928-3939, 2011, doi: 10.1016/j.jnoncrysol.2011.08.011.
[31] A. George, S. Solomon, J. K. Thomas, and A. John, “Characterizations and electrical properties of $ZrTiO_4$ ceramic,” Mater. Res. Bull., vol. 47, (11) pp. 3141-3147, 2012, doi: 10.1016/j.materresbull.2012.08.018.
[32] I. Ganesh, “A review on magnesium aluminate ($MgAl_2O_4$) spinel: synthesis, processing and applications,” Int. Mater. Rev., vol. 58, pp. 63–112, 2013, doi: 10.1179/1743280412Y.0000000001.
[33] P. A. Loiko, O. S. Dymshits, N. A. Skoptsov, A. M. Malyarevich, A. A. Zhilin, I. P. Alekseeva, M. Y. Tsenter, K. V. Bogdanov, X. Mateos, and K. V. Yumashev, “Crystallization and nonlinear optical properties of transparent glass-ceramics with $Co:Mg(Al,Ga)_2O_4$ nanocrystals for saturable absorbers of lasers at 1.6–1.7 μm,” J. Phys. Chem. Solid, vol. 103, pp. 132–141, 2017, doi: 10.1016/j.jpcs.2016.12.017.
[34] B. M. Loeffler, R. G. Burns, J. A. Tossell, D. J. Vaughan, and K. H. Johnson, “Charge transfer in lunar materials: interpretation of ultraviolet-visible spectral properties of the moon,” in: Lunar and Planetary Science Conference Proceedings, vol. 5, pp. 3007–3016, 1974.
[35] H. K. Mao and P. M. Bell, “Crystal-field effects of trivalent titanium in fassaite from the Pueblo de Allende meteorite,” Ann. Rep. Geophys. Lab., Carnegie Inst. Washington Year Book, vol. 73, pp. 488–492, 1974.
[36] D. A. Nolet, R. G. Burns, S. L. Flamm, and J. R. Besancon, “Spectra of Fe-Ti silicate glasses: implications to remote-sensing of planetary surfaces,” in: Lunar and Planetary Science Conference Proceedings, vol. 10, pp. 1775–1786, 1979.
[37] V. Vercamer, G. Lelong, H. Hijiya, Y. Kondo, L. Galoisy, and G. Calas, “Diluted Fe^{3+} in silicate glasses: structural effects of Fe-redox state and matrix composition. An optical absorption and X-band/Q-band EPR study,” J. Non-Cryst. Solids, vol. 428, pp. 138–145, 2015, doi: 10.1016/j.jnoncrysol.2015.08.010.

[38] G. H. Faye and D.C. Harris, “On the origin and pleochroism in andalusite from Brazil,” Can. Mineral., vol. 10, pp. 47–56, 1969.
[39] A. S. Marfunin, “Physics of Minerals and Inorganic Materials: an Introduction”, Springer-Verlag, Berlin, Heidelberg, New York, 1979, p. 340.
[40] J. Cardoso-Fernandes, J. Silva, M. M. Perrotta, A. Lima, A. C. Teodoro, M. A. Ribeiro, F. Dias, O. Barrès, J. Cauzid, and E. Roda-Robles, “Interpretation of the reflectance spectra of lithium (Li) minerals and pegmatites: A case study for mineralogical and lithological identification in the Fregeneda-Almendra area,” Remote Sens., vol. 13, pp. 3688, 2021, doi: 10.3390/rs13183688.
[41] R. Reisfeld, A. Kisilev, A. Buch, and M. Ish-Shalom, “Transparent glass-ceramics doped by chromium(III): Spectroscopic properties and characterization of crystalline phases,” J. Non-Cryst. Solids, vol. 91 (3), pp. 333-350, 1987, doi: 10.1016/S0022-3093(87)80344-7.
[42] M. N. Taran, M. Koch-Müller, and K. Langer, “Electronic absorption spectroscopy of natural (Fe^{2+}, Fe^{3+})-bearing spinels of spinel ss-hercynite and gahnite-hercynite solid solutions at different temperatures and high-pressures,” Phys. Chem. Miner., vol. 32, pp. 175–188, 2005, doi: 10.1007/s00269-005-0461-z.
[43] V. D’Ippolito, “Linking Crystal Chemistry and Physical Properties of Natural and Synthetic Spinels: an UV–VIS–NIR and Raman Study,” Doctoral dissertation, Sapienza Universit`a di Roma, 2013, p. 237.
[44] C. Fernandez-Martin, G. Bruno, A. Crochet, D. O. Ovono, M. Comte, and L. Hennet, “Nucleation and growth of nanocrystals in glass-ceramics: an in situ SANS perspective,” J. Am. Ceram. Soc., vol. 95 (4), pp. 1304–1312, 2012, doi: 10.1111/j.1551-2916.2012.05093.x.